Geochemistry Geophysics Geosystems G3
AN ELECTRONIC JOURNAL OF THE EARTH SCIENCES
Published by AGU and the Geochemical Society

Article
Volume 8, Number 2
13 February 2007
Q02006, doi:10.1029/2006GC001390
ISSN: 1525-2027

Temperatures in ambient mantle and plumes: Constraints from basalts, picrites, and komatiites

C. Herzberg
Department of Geological Sciences, Rutgers University, Piscataway, New Jersey, USA (herzberg@rci.rutgers.edu)

P. D. Asimow
Geological and Planetary Sciences, California Institute of Technology, Pasadena, California, USA

N. Arndt
Laboratoire de Géodynamique des Chaînes Alpines, Université Joseph Fourier à Grenoble, St. Martin d'Hères, France

Y. Niu
Department of Earth Sciences, University of Durham, Durham, UK

C. M. Lesher
Department of Earth Sciences, Laurentian University, Sudbury, Ontario, Canada

J. G. Fitton
School of GeoSciences, University of Edinburgh, Edinburgh, UK

M. J. Cheadle
Department of Geology and Geophysics, University of Wyoming, Laramie, Wyoming, USA

A. D. Saunders
Department of Geology, Leicester University, Leicester, UK

[1] Several methods have been developed to assess the thermal state of the mantle below oceanic ridges, islands, and plateaus, on the basis of the petrology and geochemistry of erupted lavas. One leads to the conclusion that mantle potential temperature (i.e., T_P) of ambient mantle below oceanic ridges is 1430°C, the same as Hawaii. Another has ridges with a large range in ambient mantle potential temperature (i.e., T_P = 1300–1570°C), comparable in some cases to hot spots (Klein and Langmuir, 1987; Langmuir et al., 1992). A third has uniformly low temperatures for ambient mantle below ridges, ~1300°C, with localized 250°C anomalies associated with mantle plumes. All methods involve assumptions and uncertainties that we critically evaluate. A new evaluation is made of parental magma compositions that would crystallize olivines with the maximum forsterite contents observed in lava flows. These are generally in good agreement with primary magma compositions calculated using the mass balance method of Herzberg and O'Hara (2002), and differences reflect the well-known effects of fractional crystallization. Results of primary magma compositions we obtain for mid-ocean ridge basalts and various oceanic islands and plateaus generally favor the third type of model but with ambient mantle potential temperatures in the range 1280–1400°C and thermal anomalies that can be 200–300°C above this background. Our results are consistent with the plume model.

Components: 22,775 words, 10 figures, 1 table.

Keywords: mantle plumes; ambient mantle temperatures; petrology; mid ocean ridge basalt.

Index Terms: 3610 Mineralogy and Petrology: Geochemical modeling (1009, 8410); 3619 Mineralogy and Petrology: Magma genesis and partial melting (1037); 3621 Mineralogy and Petrology: Mantle processes (1038).

Received 16 June 2006; **Revised** 10 October 2006; **Accepted** 13 November 2006; **Published** 13 February 2007.

Herzberg, C., P. D. Asimow, N. Arndt, Y. Niu, C. M. Lesher, J. G. Fitton, M. J. Cheadle, and A. D. Saunders (2007), Temperatures in ambient mantle and plumes: Constraints from basalts, picrites, and komatiites, *Geochem. Geophys. Geosyst.*, *8*, Q02006, doi:10.1029/2006GC001390.

1. Introduction

[2] The petrology and geochemistry of lavas at oceanic ridges, islands, and plateaus provide a record of the thermal state of the mantle where they form. We know from experimental petrology that dry hot mantle will produce magmas with higher MgO contents than mantle that is cooler. A calibration and parameterization of these laboratory data can then be applied to mafic-ultramafic volcanic rocks, and the thermal state of their source can be inferred. However, geologists sample a wide range of volcanic rocks with a diverse geochemistry that can arise by fractional crystallization [*Lewis*, 1907; *Bowen*, 1928]. The problem is how to integrate field and laboratory observations to obtain information about the temperature properties of the mantle below a volcano. In practice, this can be complex and may lead to different conclusions, resulting in the current debate about whether all mafic-ultramafic magmas can be derived from "ambient" mantle or whether some must be derived from anomalously hot mantle plumes.

[3] For example, *Foulger and Natland* [2003, p. 921] suggested that "petrological observations provide little evidence of the high eruptive temperatures required by deep plumes." Although this assertion was made with Iceland in mind, *Green et al.* [2001] used petrological calculations to conclude that primary magmas from Hawaii and mid-ocean ridge basalt (MORB) melted from mantle with a uniform potential temperature (i.e., T_P = 1430°C). This is the temperature that the solid adiabatically convecting asthenospheric mantle would have if it could reach the surface metastably without melting [*McKenzie and Bickle*, 1988]. In contrast, *Klein and Langmuir* [1987] and *Langmuir et al.* [1992] calculated a large temperature variation of ambient mantle below oceanic ridges (i.e., T_P = 1300–1570°C), with Iceland at the high end of the range. If magmas below hot ridges and hot spots are equally hot, why do we need mantle plumes? Indeed, *Anderson* [2000] cited the hot end of the range in Langmuir et al.'s models as evidence precluding the need for hot mantle plumes. In contrast, other models have favored uniformly low ambient mantle temperatures for ridges [*Shen and Forsyth*, 1995; *Presnall et al.*, 2002]. The plume model is most consistent with anomalously hot mantle temperatures beneath volcanically active ocean islands compared to ambient mantle below oceanic ridges (i.e., $\Delta T_P \cong 250$°C [*McKenzie and Bickle*, 1988; *McKenzie and O'Nions*, 1991; *Watson and McKenzie*, 1991; *Schilling*, 1991; *Herzberg and O'Hara*, 2002; *Putirka*, 2005; *Putirka et al.*, 2006]).

[4] The purpose of this paper is to determine the temperature of the mantle below volcanoes from diverse tectonic environments, and to evaluate why there are substantially different thermal models for an essentially common volcano database. We focus on the petrological and geochemical characteristics of primitive basalts, picrites, and komatiites – volcanic rocks that are variably enriched in MgO and olivine. The distribution of these rocks in oceanic ridges, islands, and plateaus permits an evaluation of temperatures in ambient and anomalous mantle, and a test of the plume hypothesis. We examine model assumptions that can contribute to uncertainties and completely different conclusions about the plume model. MORB production from ambient mantle is critical in this discussion because it provides the background reference frame for understanding all thermal anomalies.

2. Parental and Primary Magmas: Concepts and Definitions

[5] We begin this analysis by understanding the effects of fractional crystallization on the compo-

sitions of volcanic rocks from oceanic ridges and some intraplate occurrences. The goal is to first identify the parental magma, which is defined as the most magnesian liquid that can be inferred from a given rock suite in the crust. In general the parental magma is never observed directly: all erupted rocks are modified to some extent by fractional crystallization and/or mixing and crystal accumulation, but parental magma compositions can be restored by a well-defined procedure. There is widespread agreement on the essentials of this procedure [e.g., *Nisbet et al.*, 1993] although different assumptions about the details lead to a range of results. Next, we want to understand the relationship between the parental and primary magmas. A primary magma is defined as a partial melt of a mantle source which we characterize more fully below. It is the primary magma that we are most concerned about because it contains information about the thermal characteristics of the source. We emphasize that the composition of the parental magma may be the same as the primary magma. However, the primary magma may also be more primitive (i.e., higher MgO) than the parental magma if there was modification before the crystallization of the most magnesian observed phenocryst. The derivation of a primary magma solely by reconstruction from observed rocks is not a well-defined procedure and this has led to considerable divergence of opinion on the nature of primary magmas. Following *Herzberg and O'Hara* [2002], we supplement reconstruction of parental magmas with forward calculations of mantle melting to constrain primary magma compositions. A detailed example is given as a tutorial in Appendix A.

[6] Partial melts can have compositions that vary with the style of melting [*Gast*, 1968; *Shaw*, 1970; *Albarède*, 1995]. Fractional melting occurs when the melts segregate from the crystalline residue owing to the buoyancy of the melt. In batch melting, the melt does not separate from the residue until the very end when melting stops, at which point it leaves in a single homogeneous batch. Although batch melting equations correctly describe steady, one-dimensional, equilibrium porous flow [e.g., *Ribe*, 1985; *Richter*, 1986; *Spiegelman and Elliott*, 1993; *Asimow and Stolper*, 1999], it is more likely that percolation at separation velocity slow enough to maintain equilibrium only carries a very small amount of melt [*McKenzie*, 1984, 2000], with the bulk of melt transport through pathways that prevent continuous equilibration between melts and residues [*Kelemen et al.*, 1997]. Batch melting is often interpreted by experimental petrologists if they observe a magma that is multiply saturated in crystalline phases in a high-pressure laboratory experiment [*Green et al.*, 2001]. However, fractional melts can also display the properties of multiple saturation [*Asimow and Longhi*, 2004]. In the case of melting below oceanic ridges, trace element data in clinopyroxene from abyssal peridotites cannot be reconciled with a batch melting model and rather require something approaching fractional melting [*Johnson et al.*, 1990]. We contribute to this discussion by showing that batch melting is unlikely for MORB because the melt fractions are too high and by illustrating the consequences of fractional melting for inference of primary magma composition.

[7] When a mantle source rock is partially melted, it is the liquid-crystal density difference that provides the principal driving force for melt segregation and hence fractional melting, and this occurs at low pressures appropriate for Phanerozoic magmatism. However, in the Proterozoic and Archean, this issue may be more complex in those cases where partial melting occurred at pressures in excess of 8 GPa [*Sproule et al.*, 2002; *Herzberg*, 2004a] because crystal-liquid densities become similar [*Agee*, 1998]. Although batch melting might be a factor for Archean komatiite generation at some stage [*Herzberg*, 2004a], we focus on the Phanerozoic where fractional melting is more important.

[8] Fractional melting can be approximated as a series of small increments of equilibrium melting followed by extraction of all or most of the melt. Melting begins at a specified pressure, the instantaneous parcel of melt is in equilibrium with its residue, and it is subsequently removed. The residue changes in composition owing to this melt removal, and it moves upward where it melts to yield another instantaneous parcel of liquid, a process that is repeated many times until melting terminates at some lower pressure. There are two kinds of primary magmas of fractional melting. In the first, an instantaneous parcel of melt can escape directly to the surface. In the second, the instantaneous parcels of melt mix with one another, and the composition of the "pooled" or "aggregated" melt is the average composition of all the melt fractions [*Shaw*, 1970].

[9] An aggregate melt is not in equilibrium with its residue; only the final drop of instantaneous melt extracted is in equilibrium with the residue. A more complete and quantitative discussion of relationships among melts, residues and initial source

compositions can be found elsewhere [*Herzberg*, 2004a]. The aggregated melt is the most important type of primary magma because its composition is most representative of the bulk composition of the oceanic crust. Both types provide temperature information of melting, and examples are given below. We have not explicitly accounted for partial melt-rock reaction during melt migration. It is expected to generate melts intermediate between the perfect fractional (no reaction) and batch (complete equilibrium during migration) end-members.

[10] Numerical models of perfect fractional melting can be obtained either by iterative solutions to the equation for batch melting or by mass balance solutions to the equation for accumulated fractional melting [*Shaw*, 1970; *Albarède*, 1995]. Both methods give the same results (Appendix A), and the solutions reported by *Herzberg and O'Hara* [2002] will be used here. Results for major elements are not significantly affected by including a small trapped melt fraction within a residual porosity.

[11] Primary magmas and their solid and liquid derivatives make up the oceanic crust [*Elthon*, 1979]. The compositions of the bulk oceanic crust and the primary magma formed by accumulated fractional melting will be identical if fractional crystallization does not occur in the mantle. Parental and primary magmas will only be identical in composition if there is no heat loss and no olivine crystallization anywhere during magma transport from the mantle source to the volcano [*O'Hara*, 1968]. Fractional crystallization changes primary magmas to parental magmas with lower MgO contents. There is a considerable body of evidence that indicates it occurs in lava flows and shallow level magma chambers that solidify as dikes and sills [*O'Hara*, 1968]. However, it can also occur in the mantle below oceanic ridges [*Grove et al.*, 1992; *Niu*, 1997; *Coogan et al.*, 2001; *Herzberg*, 2004b; *Schwartz et al.*, 2005], Réunion [*Albarède et al.*, 1997], and west Greenland [*Larsen and Pedersen*, 2000].

2.1. Calculation of Parental Magma Compositions: Method and Examples

[12] In order to restore the parental magma composition, the process of fractional crystallization is inverted. This examination begins with the case of low-pressure fractional crystallization of olivine. A discussion follows with more complex cases involving plagioclase and augite, and high-pressure crystallization. We will examine 3 cases that are representative of many volcanoes produced by decompression melting of the Earth's mantle, and use them to illustrate the computational method for restoring parental magma composition (Figure 1a). We examine basalts from the Siqueiros Transform that offsets the East Pacific Rise (EPR) [*Perfit et al.*, 1996] and the Ontong Java Plateau [*Fitton and Godard*, 2004]. We also examine the picrites and komatiites of Cretaceous age from the island of Gorgona [*Echeverria*, 1980; *Aitken and Echeverria*, 1984; *Echeverria and Aitken*, 1986; *Kerr et al.*, 1996; *Arndt et al.*, 1997; *Révillon et al.*, 1999, 2000].

[13] For Gorgona, the terms "picrite" and "komatiite" have been used to describe hyaloclastic volcanic rocks without spinifex textures and lava flows with spinifex textures, respectively. Olivine fractionation and accumulations control the geochemistry of each population, resulting in lavas with a wide range of MgO contents at nearly constant FeO (Figure 1a). This process can be described with a variety of computational procedures, all of which provide information about parental magma composition [*Irvine*, 1977; *Pearce*, 1978; *Hanson and Langmuir*, 1978; *Langmuir and Hanson*, 1980; *Albarède*, 1992; *Nisbet et al.*, 1993].

[14] Before a parental magma composition can be calculated, it is necessary to know the composition of olivine that will crystallize from a liquid. It is determined using the Fe-Mg exchange coefficient $K_D = (FeO/MgO)^{ol}/(FeO/MgO)^{L}$, first introduced by *Roeder and Emslie*, [1970]. The model of *Toplis* [2005] is used here to describe the effects of temperature, pressure, and composition on K_D. We assume olivine crystallization occurs at near atmospheric pressure. At high pressures within the melting regime, the model of *Toplis* [2005] is similar to that of *Herzberg and O'Hara* [2002]; pressure effects on K_D will be examined below. The temperature at which olivine crystallizes, which is required in the Toplis K_D, is calculated from the method of *Beattie* [1993], also discussed below. For the case of near-surface crystallization considered in Figure 1a, the *Toplis* [2005] parameterization yields K_D that is very similar to the commonly used model of *Ford et al.* [1983]. Each green line in Figure 1a shows an array of liquid compositions that precipitate olivine with a given Fo content at the surface. The composition of olivine is expressed as Mg number (Mg # = 100 MgO/(MgO + FeO)) molar although, for convenience, we use the term forsterite content (Fo = mole fraction Mg_2SiO_4). For naturally occur-

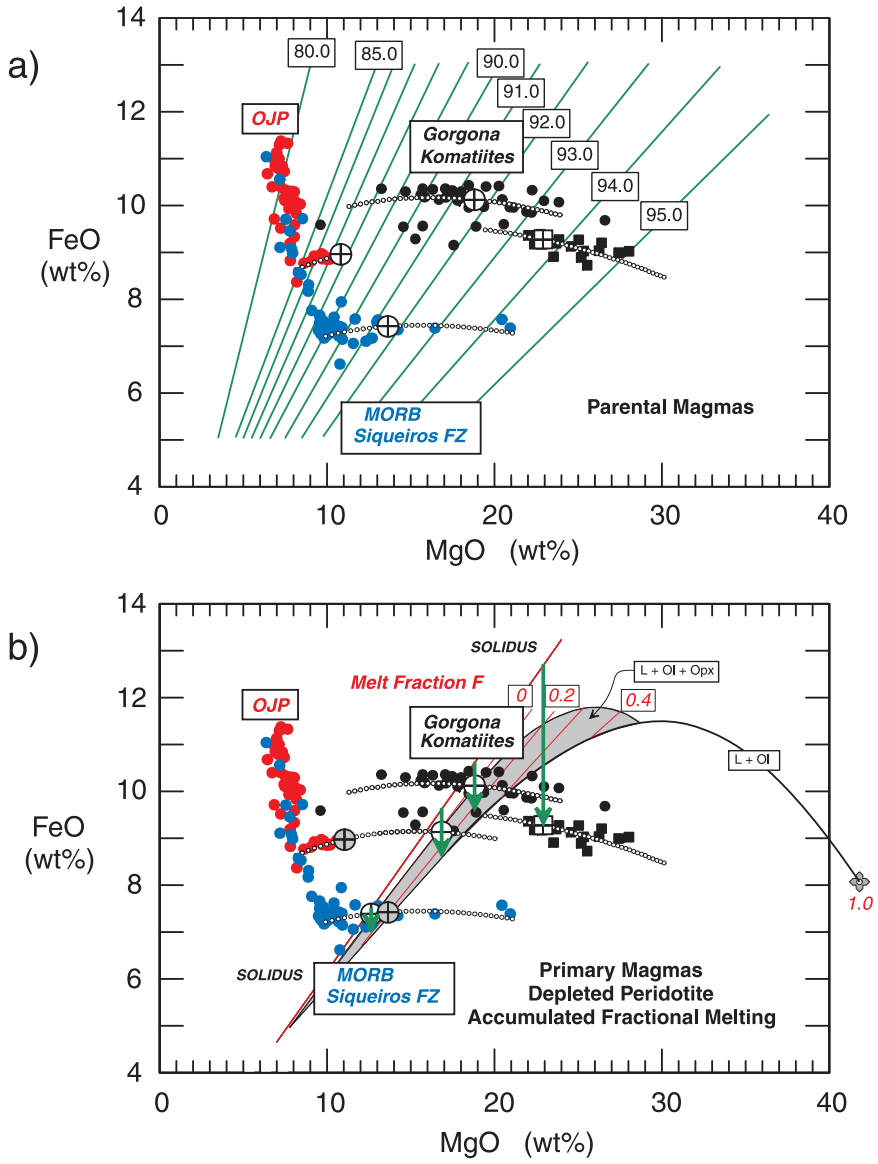

Figure 1. (a) Illustration showing the method for computing parental magma compositions for basalts from the Ontong Java Plateau and the Siqueiros Fracture Zone (East Pacific Rise) and komatiites and picrites from Gorgona. Green lines are Fo contents of olivine (100 MgO/(MgO + FeO) molar) at 1 atm calculated from the K_D model of *Toplis* [2005] at 1 atm. Arrays of small circles indicate liquid compositions produced by addition, i.e., of olivine into a representative lava composition. Crosses in circles indicate parental magma, which is defined by the coincidence of an olivine addition array with an olivine phenocryst composition having the maximum Fo content (target olivine). Black, red, and blue circles are whole rock and glass data for Gorgona komatiites, Ontong Java Plateau, and MORB from the Siqueiros FZ. Olivine was added to Gorgona sample 149 [*Aitken and Echeverria*, 1984], OJP sample 1187-8 [*Fitton and Godard*, 2004], and Siqueiros sample ALV2384-007B [*Perfit et al.*, 1996]. (b) Illustration showing the method for computing primary magma composition of the lavas in Figure 1a. Red lines indicate FeO and MgO contents of accumulated fractional melts of depleted peridotite at the melt fractions F shown [*Herzberg and O'Hara*, 2002]. Green arrows illustrate the approximate range of instantaneous fractional melts that, when mixed together, produce the accumulated fractional melts. Crosses in gray circles for MORB and Ontong Java Plateau are the parental magmas from Figure 1a. Crosses in white circles indicate primary magmas formed at the same melt fractions as those given in Figure 2. MgO contents do not change much with decompression because dT/dP of isopleths of MgO in partial melts of peridotite approximately parallel the adiabatic gradient [*Herzberg and O'Hara*, 2002] (but see small changes in Appendix A for fertile peridotite). Black, red, and blue circles are whole rock and glass data from Figure 1a.

ring lavas, we need to know how much of the total iron can be exchanged with FeO in olivine (i.e., Fe^{2+} versus Fe^{3+}). For MORB glasses, we will use $Fe^{2+}/\Sigma Fe = 0.93$ from *Christie et al.* [1986]. For Gorgona and Ontong Java lavas, we assume $Fe^{2+}/\Sigma Fe = 0.90$, based on analogy with early Kilauea glass analyses [*Wright et al.*, 1975]. This is reasonably consistent with recent ferrous iron measurements on Mauna Loa lavas, which demonstrate that rapidly quenched lavas record an oxidation state close to the magnetite-wüstite buffer, with $Fe^{3+}/\Sigma Fe$ as low as 0.06 [*Rhodes and Vollinger*, 2005].

[15] Now that the composition of olivine can be computed, we use the following procedure to calculate parental magma composition. A representative lava composition is selected, its equilibrium olivine composition is computed, and olivine is then added or subtracted incrementally. This procedure generates the subhorizontal curves in Figure 1a, and is a good way to simulate and visualize fractional crystallization of olivine. The parental magma composition is identified as the one with a calculated olivine composition that is the same as the observed olivine having the highest Mg number, the target olivine composition. That is, the parental magma is defined as the most primitive magma that can be inferred from direct observation of a rock suite and the observation that retains the earliest evidence of differentiation is the most magnesian olivine phenocryst composition. As we discuss below, the choice of target olivine composition is an important source of uncertainty and disagreement in this calculation. One must define a suite of rocks that are considered to be associated and use the most magnesian phenocryst in any one of those rocks as a target for back correction of all the rocks in the suite; definition of suites can be somewhat arbitrary. Furthermore, by definition the maximum Mg number observed in a phenocrysts is an outlier and ties the entire calculation to what may in fact be an anomalous sample. Finally, we argue below that one consequence of fractional melting is that highly magnesian olivines may not in fact be phenocrysts associated with the direct parent of a measured liquid composition.

[16] The parental magma for the Gorgona komatiites contained 19% MgO, and this would crystallize olivine with Fo 91.5, the maximum observed. Fractional crystallization of olivine from this parental magma produced derivative liquids with MgO < 19%, and these crystallized olivine with Fo < 91.5. Accumulation of olivine produced lavas with more than 19% MgO. While accumulation may be conceptually different from the reverse of fractional crystallization if the accumulated olivines are out of equilibrium with the liquids, the differences are small and we neglect this effect. For the Gorgona picrites, the parental magma contained 23% MgO and crystallized olivine with Fo 93.6.

[17] Plagioclase or plagioclase + augite crystallize together with olivine when the MgO content of the liquid drops below the 7–10 wt % range, and this causes the FeO content of the liquid to go up, yielding the negative FeO-MgO trend that is common in tholeiitic oceanic basalts (Figure 1a). Lavas from the Ontong Java Plateau and the East Pacific Rise (Siqueiros MORB) are good examples. However, they also have an important population of primitive lavas containing olivine as the sole phenocryst phase, and to these olivine can be added to derive the parental magma composition. The parental magma for the Ontong Java Plateau had 11% MgO, and crystallized olivine with Fo 87.7, the observed maximum [*Sano and Yamashita*, 2004]. The parental magma for Siqueiros MORB contained 14% MgO, based on maximum Fo 91.5 olivine [*Perfit et al.*, 1996]. We note that, in the absence of lavas sufficiently primitive to only crystallize olivine, the lowest observed FeO among multiply saturated lavas in a suite provides an upper bound on the FeO and hence MgO contents of the parental magma.

[18] It is assumed that olivine phenocrysts in lava flows crystallize at near surface conditions. However, some olivine phenocrysts might also precipitate in the mantle and be carried to the crust. This is indicated by clinopyroxene phenocrysts in lavas from northern Iceland, which have compositions that reflect crystallization in the mantle [*Slater et al.*, 2001]. Computing primary magma compositions using low-pressure K_D but targeted to an olivine composition that actually crystallized in the mantle will result in MgO contents that are too low by 1–2% based on the K_D models of *Toplis* [2005] and *Herzberg and O'Hara* [2002]. This will propagate to magmatic temperatures that are too low by 20–40°C. We assume near-surface conditions in the calculations because, unlike clinopyroxene, we have no way to uniquely constrain the depth at which olivine crystallizes.

2.2. Calculation of Primary Magma Compositions: Method and Examples

[19] It is now necessary to evaluate the relationship between the parental magma compositions shown

in Figure 1a and the associated primary magma compositions extracted from the mantle source. In order to proceed, we need to know the mineralogy and composition of the source lithology, and the compositions of all partial melts that might be derived from it. Peridotite and eclogite/pyroxenite lithologies are likely candidates, and both display a considerable range of compositions. Progress in understanding criteria for source lithological identification is being made, and it has been proposed that both peridotite and pyroxenite sources contribute to magmatism below Hawaii [*Sobolev et al.*, 2005; *Herzberg*, 2006]. For the purposes of this work, we seek those constraints on source temperature that are most independent of assumptions about source lithology.

[20] Gorgona lavas considered in Figure 1 contain low NiO and high CaO contents that are indicative of a peridotite source [*Sobolev et al.*, 2005; *Herzberg*, 2006]. Ontong Java plateau lavas contain major elements that indicate a peridotite source, but NiO is somewhat high and a possible role of pyroxenite melting is discussed in the Appendix A. A peridotite source is assumed for Siqueiros MORB. Trace element depletions in Gorgona [*Arndt et al.*, 1997] and Siquieros MORB [*Perfit et al.*, 1996] indicate the peridotite source is depleted. In contrast, Ontong Java Plateau lavas display the properties of melting from a fertile peridotite source [*Fitton and Godard*, 2004; *Tejada et al.*, 2004; *Herzberg*, 2004c]. Uncertainties about the exact peridotite composition are not important in this case because the MgO content of primary magmas from depleted and fertile peridotite sources are very similar [*Herzberg and O'Hara*, 2002] (Appendix A).

[21] The method to calculate primary magma composition [*Herzberg and O'Hara*, 2002] is illustrated as a tutorial in Appendix A. PRIMELT1 software is now available for doing the calculations. First, olivine is added and/or subtracted from a representative lava composition in the usual way. This produces an array of possible primary magma compositions as before, an inverse model. This array is then compared with the full range of accumulated partial melts for depleted peridotite [*Herzberg and O'Hara*, 2002], a forward model (Figure 1b). How do we obtain a solution that is unique to both forward and inverse models? Instead of targeting to the liquid that matches the maximum Fo content of an olivine phenocryst in a lava, it is targeted to the melt fraction (F) of the primary magma as discussed in more detail in Appendix A. Specifically, a unique solution is obtained when a liquid along the olivine addition–subtraction array displays a common melt fraction in both FeO-MgO space (Figure 1b) and projection space (Figure 2) for accumulated fractional melts. The projection is a two-dimensional representation of a 12-component chemical system [*O'Hara*, 1968], but topologically, the family of liquids derived by batch melting of a given source must form a surface (a two-dimensional membrane) in a space of any dimensionality (this is a consequence of Duhem's theorem) and the surfaces for accumulated fractional melts generally have similar topology. Hence unique solutions can in principle be found by comparing melt fractions in FeO-MgO with any two-dimensional plot of liquid compositions that does not show much crossing of melt fraction contours, e.g., MgO-SiO_2 space (see Appendix A). This is a complete mass balance solution to the primary magma problem given an assumption of source composition, and adequate experimental data to define the partial melt compositions. This method of calculating primary magma composition is independent of observed olivine phenocryst composition and avoids the confounding issues with choice of target olivine composition encountered above in the course of calculating parental magmas. Examples of this method are now given for a depleted peridotite source, and the results are similar to those obtained for fertile peridotite (Appendix A).

[22] For Ontong Java Plateau (OJP) basalts, the parental magma is too low in MgO to be a primary magma of depleted peridotite under any condition of fractional melting (Figure 1b). The same holds true for batch or accumulated fractional melting of any peridotite source. To obtain the primary magma composition, we add olivine in the usual way. However, instead of targeting the calculation to the maximum Fo observed in a sampled phenocryst (i.e., 87), it is targeted to a melt fraction of 0.11 in both FeO-MgO (Figure 1b) and projection space (Figure 2). This method gives a primary accumulated OJP magma with 17% MgO [*Herzberg*, 2004c]; it would crystallize olivine with Fo 91.4 at the surface. Addition of an extra 1.8 weight percent olivine would raise the MgO to 18%. However, this is not an acceptable solution because the liquid will read a melt fraction of 0.20 in FeO-MgO space, but 0.12 in projection space, violating the requirement of internal consistency and mass balance. The method is accurate because small variations in the MgO content of a primary magma require large variations in melt fraction,

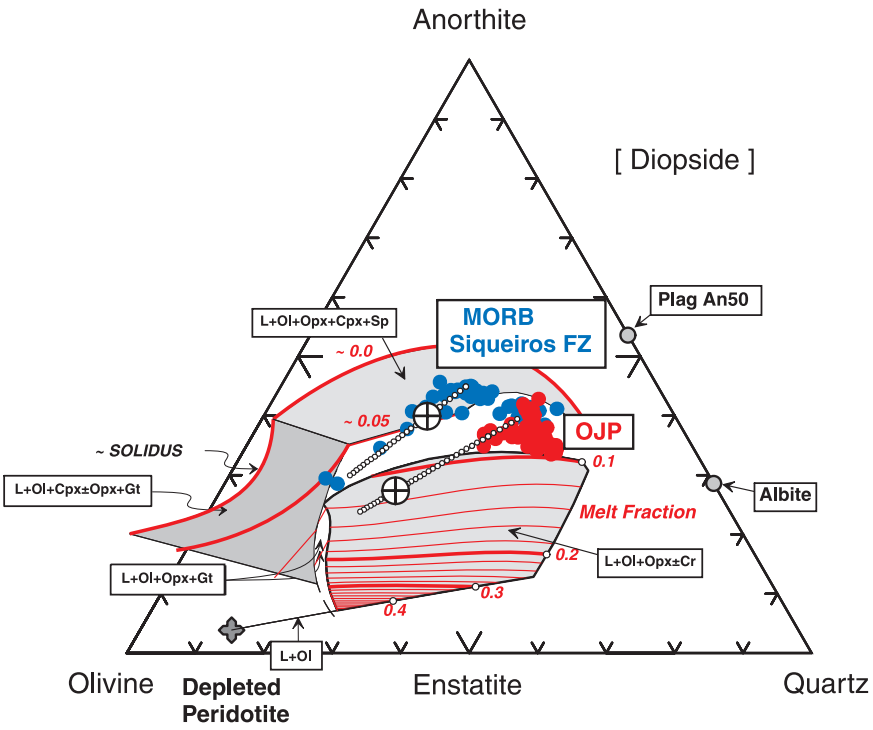

Figure 2. A projection of liquid compositions (mol %) of depleted mantle peridotite from Diopside (CMS_2) and $Na_2O \bullet Si_3O_6$ and $K_2O \bullet Si_3O_6$ into the plane olivine-anorthite-silica [*Herzberg and O'Hara*, 2002]. Red lines indicate contours of equal melt fraction, as shown also in Figure 1b of *Herzberg and O'Hara* [2002]. Gorgona lava compositions are not shown to preserve clarity, but these can be seen Figure 10 of *Herzberg and O'Hara* [2002]. Crosses in white circles indicate primary magmas formed at the same melt fractions as those given in Figure 1b. Arrays of small circles radial from the olivine vertex are olivine fractionation/addition trends. All wt % compositions are converted to mol %. Projection coordinates are calculated in the following way: olivine = $-1.5TiO_2 + 0.5Al_2O_3 + 0.5Cr_2O_3 + 0.5FeO + 0.5MnO + 0.5MgO - 0.5CaO - 0.5Na_2O + 3.0K_2O + 0.5NiO$, anorthite = $1.0TiO_2 + 1.0Al_2O_3 + 1.0Cr_2O_3$, quartz = $1.0SiO_2 - 0.5Al_2O_3 - 0.5Cr_2O_3 - 0.5FeO - 0.5MnO - 0.5MgO - 1.5CaO - 3.0Na_2O - 3.0K_2O - 0.5NiO$.

and these can be independently evaluated using other plots (Figure 2 and Appendix A).

[23] For Gorgona komatiites, the primary magma composition contains 19% MgO and the melt fraction is 0.11 in both FeO-MgO and projection space. The primary magma (Figure 1b) is identical in composition to the parental magma (Figure 1a). This is an example where a primary magma can directly exit the mantle source and erupt as the parental magma, crystallizing olivine with Fo 91.5. Note, however, that the primary magmas derived for Ontong Java and for Gorgona komatiites are not the same despite sharing a melt fraction and a Mg number; the Gorgona model primary liquid has higher MgO and FeO and implies melting at higher pressure and temperature.

[24] For Gorgona picrites, the parental magma with 23% MgO does not coincide with any possible accumulated fractional melt composition in Figure 1b. Although not shown, this also holds true for all other possible melting scenarios. That is, the parental magma for Gorgona picrites cannot form by either batch or accumulated fractional melting of any peridotite source composition. How do we interpret this parental magma? *Arndt et al.* [1997] proposed that the extreme depletions in incompatible element concentrations can be explained if the picrites crystallized from late stage fractional melts. This is the first type of primary magma discussed above, and it yields useful information about the temperature of the source. This model will be examined more carefully below.

[25] For MORB from the Siqueiros Transform, the primary magma contains 13% MgO and will form at a melt fraction of 0.05. This result compares favorably with the 0.06 melt fraction inferred by *Workman and Hart* [2005] from trace element modeling of a depleted peridotite source and by

Asimow and Langmuir [2003] from forward models of melting regimes in the presence of small amounts of water in the source. Our primary MORB magma would precipitate olivine with Fo 91.0 at the surface, slightly lower than the observed Fo max of 91.5. Addition of a small amount of olivine can yield another possible primary magma solution with 14% MgO, and this would crystallize Fo 91.5 olivine, the same as our parental magma (Figure 1a). However, this alternate primary magma solution is not acceptable because the melt fraction would be 0.20 in FeO-MgO space and 0.05 in projection space. Our "parental magma" has a higher MgO content than the primary magma, a paradox that will be examined next.

2.3. Olivine Composition Variations During Partial Melting

[26] Some lavas contain highly forsteritic olivine phenocrysts, and it is useful to understand how these can form. This is especially important for interpretations of calculated parental magma compositions.

[27] Figure 1b illustrates how fractional melting can produce compositional variations of olivine. FeO decreases during decompression melting and, although MgO also varies, the changes are small [*Herzberg and O'Hara*, 2002] (Appendix A) and we will keep it constant for simplicity. The olivine compositions are those that would crystallize from fractional melts at the surface. As instantaneous fractional melts become depleted in FeO with advanced melting, their equilibrium olivine crystals develop elevated Fo contents. Olivine will have about Fo 91 for near−solidus melts deepest in the melting column (Figure 1b). However, for end stage fractional melts that form at the highest levels in the melting regime, olivine can have Fo 93.6. As these melts form closest to the surface, opportunities exist for them to avoid mixing with other increments of fractional melt and erupt as primary magmas where Fo-rich olivines can crystallize in abundance. This model provides a good description for the Gorgona picrites; it is no surprise that such melts are also strongly depleted in incompatible elements [*Arndt et al.*, 1997]. Gorgona picrites are an extreme example, but the eruption of advanced stage fractional melts might also explain some very depleted picrites found on the Reykjanes Peninsula [*Fitton et al.*, 2003]. In contrast, Fo 91.5 olivine crystallized from the Gorgona komatite primary magma, which has all the properties of being a well-mixed aggregate melt (Figure 1b).

[28] Crystal growth can entomb droplets of instantaneous fractional melts and preserve them as tiny melt inclusions before they become part of the blend. This is a plausible explanation for the occurrence of olivine-hosted melt inclusions with extreme geochemical variability [*Slater et al.*, 2001; *Maclennan et al.*, 2003]. The Gorgona picrites case is clear because the high-Fo olivines are found in the late stage fractional melts from which they crystallized; little or no mixing has occurred. However, crystallization and mixing scenarios are possible that would cause olivine phenocrysts from advanced stage melts to occur in a well-mixed aggregate magma (possibly together with olivines that crystallized after the mixing). Should this occur, use of the Fo-rich olivine phenocrysts to calculate a magma composition parental to the aggregate liquid can yield MgO contents that are too high. This explanation provides a resolution to the Siqueiros MORB paradox discussed above.

[29] Clearly, distinguishing Fo-rich olivines of end stage and accumulated fractional melts is not always straightforward. Questions concerning the provenance of olivine become an issue in petrological models that make no distinction between primary and parental magmas [*Green et al.*, 2001]. Sometimes the magmas are similar in composition, but in other cases they are not (Figures 1a and 1b).

3. Parental and Primary Magmas From Different Tectonic Environments

[30] The previous discussion used several geological examples to show how parental and primary magmas can be calculated. This approach is now extended to include a larger global data set from different tectonic environments, and results are shown in Figure 3.

[31] All primary magmas are for the case of accumulated fractional melting of both depleted and fertile peridotite sources. Primary magmas for Gorgona, Ontong Java, and EPR MORB from the Siqueiros Transform are the same as those discussed above for Figure 1b. Those for the Tertiary picrites from Baffin Island and West Greenland have been reported previously [*Herzberg and O'Hara*, 2002]. For lavas from Theistareykir and Kistufell in Iceland, CaO is somewhat greater than

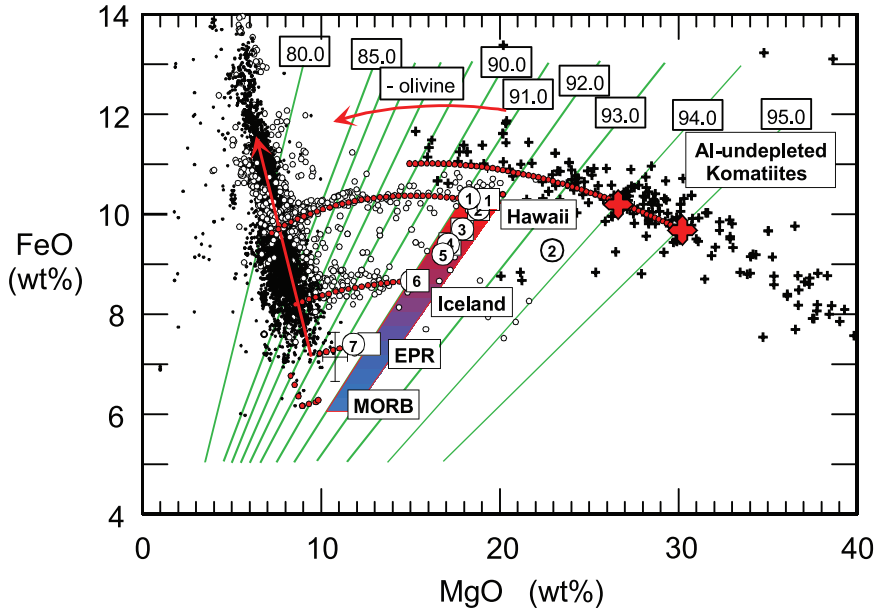

Figure 3. MgO and FeO contents of parental and primary magmas. Circles and squares numbered 1 to 7 are primary magma compositions estimated for fertile and depleted peridotite sources, respectively, as described in the text: 1, Mauna Kea; 2, Gorgona komatiites; 3, Baffin Island; 4, West Greenland; 5, Ontong Java Plateau; 6, Theistareykir, Iceland; 7, MORB from Siqueiros transform fault of EPR. Color-coded array indicates parental magmas that will crystallize olivine with Fo 91–92 at the surface. Small black dots indicate MORB glasses from the Mid-Atlantic Ridge (MAR) and East Pacific Rise (EPR) (Petrological Database of the Ocean Floor (PETDB), http://www.petdb.org). Open circles indicate lavas from Kilauea, Hawaii [*Clague et al.*, 1991; *Norman and Garcia*, 1999; *Murata and Richter*, 1966; *Wright*, 1972, 1973; *Wright and Fiske*, 1971; *Wright et al.*, 1975], and Theistareykir, Iceland [*Slater et al.*, 2001; *Maclennan et al.*, 2003]. Crosses indicate Archean Al-undepleted komatiites [*Bickle et al.*, 1975, 1993; *Nisbet et al.*, 1977, 1987; *Lesher and Arndt*, 1995; *Lahaye and Arndt*, 1996]. Small red circles indicate incremental additions and subtractions of olivine for Archean komatiites, Hawaii, Iceland, and EPR, and incremental additions of troctolite (olivine + plagioclase) for MAR. Red crosses indicate parental magma of Archean komatiite, based on olivine phenocrysts with Fo 94–95 [*Arndt*, 1986a; *Barnes et al.*, 1988; *Nisbet et al.*, 1993; *Lesher and Arndt*, 1995]. Only FeO that is exchangeable with olivine is considered, that being FeO rather than FeO_T (i.e., FeO + $0.9Fe_2O_3$). Wet chemical analysis gives $Fe^{3+}/\Sigma Fe$ of 0.07 for MORB [*Christie et al.*, 1986] and 0.10 for Kilauea [*Wright et al.*, 1975]. Mossbauer spectroscopy gives $Fe^{3+}/\Sigma Fe$ of 0.07 for Icelandic lavas [*Breddam*, 2002]. For Al-undepleted komatiites, we assume $Fe^{3+}/\Sigma Fe = 0.05$; increasing $Fe^{3+}/\Sigma Fe$ to 0.15 will lower MgO in parental magma from 30 to 28%. Arrays of small red circles indicate liquid compositions produced by subtraction of olivine from the primary magmas. The large red arrow running through the black dots shows the effect of augite and plagioclase fractionation on elevating FeO.

or equal to those of primary magmas of a peridotite source [*Herzberg*, 2006], but primary magmas calculated for both are very similar and range from 14 to 16% MgO. Primary magmas shown for Hawaii have been computed from data from Mauna Kea reported by *Frey et al.* [1991] and *Sobolev and Nikogosian* [1994]; these samples exhibit several geochemical criteria that indicate melting from a peridotite source lithology [*Sobolev et al.*, 2005; *Herzberg*, 2006], and they contain 18–19% MgO [*Herzberg*, 2006].

[32] What is most notable about Figure 3 is that all calculated primary magma compositions for the oceanic island basalt (OIB) cases are predicted to crystallize olivine at the surface with ~Fo 91.5. This coincides with observed maximum Fo contents of 91–92 shown in Figure 4 for parental magmas from Hawaii, present-day Iceland, and Gorgona komatiites. For MORB, observed maximum Fo contents are also 91–92, slightly higher than our model Fo 91.0; this difference was discussed above and will be revisited below. It is clear that in many cases the parental magmas identifiable from collected samples are nearly primary. In contrast, the Ontong Java Plateau provides a good example of primary magma modification in magma chambers or mantle conduit walls (Figure 1).

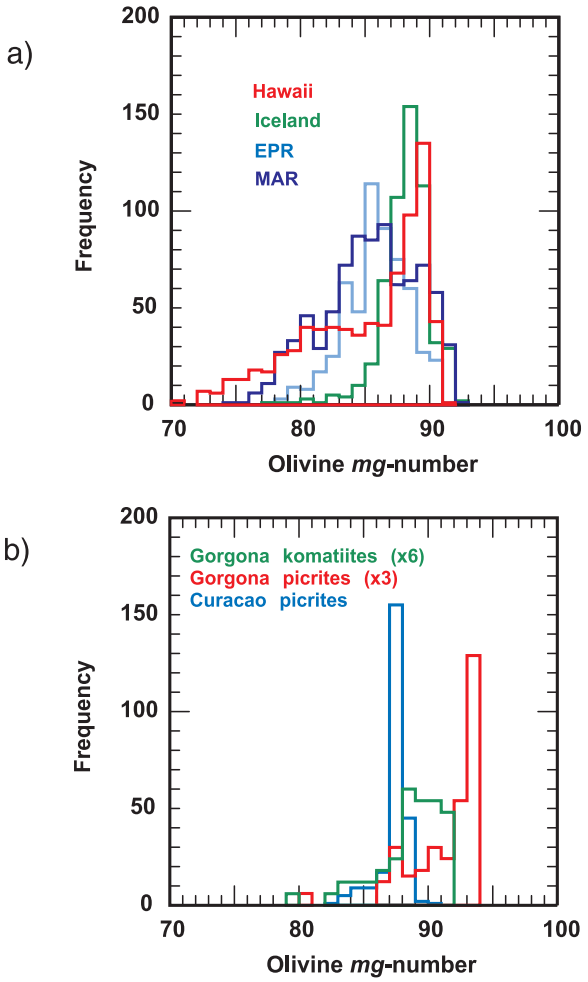

Figure 4. (a) Olivine phenocryst Mg numbers (i.e., MgO/(MgO + FeO) in mol %). Hawaii, 751 analyses from Kilauea, Mauna Loa and Mauna Kea volcanoes [*Norman and Garcia*, 1999; GEOROC, http://georoc.mpch-mainz.gwdg.de/georoc; M. Baker, personal communication, 2004]. Iceland, 549 analyses from Theistareykir province [*Slater et al.*, 2001; *Maclennan et al.*, 2003]. East Pacific Rise (EPR) and Mid-Atlantic Ridge (MAR), 587 EPR and 828 MAR analyses (PETDB; http://www.petdb.org). Most olivines from the MAR with Fo 91–92 are from a segment of the ridge closest to the Azores platform. (b) Olivine phenocryst Mg numbers (i.e., MgO/(MgO + FeO) in mol %). Gorgona and Curaçao data sources are from *Révillon et al.* [2000] and *Kerr et al.* [1996].

[33] Figure 4 shows histograms of olivine composition from these locations. An important conclusion to be drawn from Figures 3 and 4 is that widely different primary magma compositions can crystallize olivine of the same composition, Fo 91–92. The FeO-MgO primary magma array in Figure 3 applies to a wide range of tectonic environments. MORB from ambient mantle has 10–13% MgO, color-coded blue; a more detailed discussion follows. In contrast, primary magmas from Hawaii and Gorgona can have 18–23% MgO (Figure 3). Between these extremes are a range of intermediate possibilities as displayed by primary magmas from Iceland and the Ontong Java Plateau. We demonstrate next that this range has been produced by variable temperatures of mantle melting.

4. Magmatic Temperatures

[34] The 1-atm liquidus crystallization temperatures of the primary magmas identified in Figure 3 have been calculated using the method of *Beattie* [1993], and these are shown in Figure 5. If these primary magmas reached the surface they would erupt at temperatures not far from their 1-atm liquidus temperatures. Some high-flux magmas may become superheated during their ascent from their source to the surface [*Lewis and Williams*, 1973; *Lesher and Groves*, 1986], and these would erupt at temperatures above their liquidus. Most magmas, however, lose heat to their surroundings and partially crystallize; this is likely to be most problematic in low flux situations such as oceanic ridges, but it can also apply to intraplate occurrences. Partial crystallization in the crust and/or mantle will produce differentiated magmas with eruption and liquidus temperatures that are always lower than those of the primary magma. Furthermore, liquidus temperatures are always lower than potential temperatures as shown in Figure 5. Uncertainties in temperature are discussed below.

[35] Primary magmas from oceanic ridges have the lowest MgO and FeO contents (10–3% and 6–7%, respectively) and anhydrous eruption temperatures (1200–1300°C). Hawaiian parental and primary magmas can have the highest MgO and FeO contents (18–19% and 10–11%, respectively) and anhydrous eruption temperatures (1400–1450°C) of recent lavas. The parental magma of Cretaceous Gorgona picrites has still higher MgO contents (23%) and the highest eruption temperature (1500°C) of any Phanerozoic lava. Archean aluminum undepleted komatiites with 27–30% MgO were even hotter and would have erupted at ~1600°C, in good agreement with independent estimates based on 31% MgO for chilled komatiites from Kambalda [*Lesher and Arndt*, 1995]. Primary eruption temperatures therefore range from ~1200°C for MORB to 1500°C for Phanerozoic primary magmas, and >1600°C if Archean lavas are included. Clearly, some lavas were far hotter than others.

[36] Are hot spots being confused with wet spots? As long as saturation is not reached, water behaves like an incompatible element and, as for any other incompatible element, its presence lowers crystallization temperatures [e.g., *Falloon and Danyushevsky*, 2000; *Asimow et al.*, 2004]. Ratios such as H_2O/Ce are essentially constant for MORB and OIB within specific regions [*Michael*, 1995; *Dixon and Clague*, 2001; *Dixon et al.*, 2002; *Danyushevsky et al.*, 2000], and water depresses the freezing point of basaltic liquids slightly more efficiently than some elements with a heavier atomic weight. The effects of water have been evaluated by establishing how various amounts of dissolved magmatic water concentrations [*Sobolev and Chassidon*, 1996; *Dixon and Clague*, 2001; *Michael*, 1999; *Danyushevsky et al.*, 2000; *Danyushevsky*, 2001; *Nichols et al.*, 2002; *Roberge et al.*, 2004] suppress the liquidus temperature [*Falloon and Danyushevsky*, 2000], and results are included in Figure 5.

[37] Normal MORB contains ~0.04–0.20% H_2O [*Michael*, 1995; *Sobolev and Chassidon*, 1996; *Danyushevsky*, 2001], an amount that lowers olivine crystallization temperatures by about 24–42°C compared to a perfectly anhydrous system [*Falloon and Danyushevsky*, 2000]. Primitive glasses from Iceland and the Reykjanes Ridge contain 0.15–0.30% H_2O [*Nichols et al.*, 2002] which lowers their crystallization temperatures by 38–49°C, not very different from MORB (Figure 5). *Dixon and Clague* [2001] estimated that a Kilauea glass with 14.8% MgO contained 0.40% H_2O and from this we calculate that a primary magma with 19% MgO would contain ~0.35% H_2O. Its olivine liquidus temperatures will be suppressed by ~51°C (Figure 5), only slightly more than that of NMORB. Even when water is taken into account, the parental and primary melts of Hawaii, and its mantle source, are undoubtedly hot (Figure 5).

[38] Geochemical and isotopic evidence indicates the komatiites from Gorgona Island formed by fractional melting [*Arndt et al.*, 1997]. Field evidence, although complex, points to an intraplate oceanic setting [*Kerr et al.*, 1996]. If the Gorgona picrites had the same H_2O/Ce ratio as oceanic basalts, ~200, their low Ce contents of 0.3 to 0.7 ppm [*Arndt et al.*, 1997] yield exceedingly low H_2O contents of around 0.006 to 0.014%. The high MgO contents of these magmas cannot be attributed to the melting of a low-temperature hydrous source. The Gorgona picrite primary magma has a much higher MgO content than the Gorgona komatiite primary magma, indicating either the plume was superheated or the two magma types did not form by melting along a common vertical streamline. The picrites might have emerged out of the plume axis and near the top, whereas the komatiites might have come from an off-axis position that was cooler.

5. Mantle Potential Temperatures

[39] Mantle potential temperatures (i.e., T_P) calculated for peridotite source melting using the method of *McKenzie and Bickle* [1988] are shown in Figure 5. It is 1280 to 1400°C for MORB magmas with 10–13% MgO, in good agreement with previous estimates for ambient mantle [*McKenzie and Bickle*, 1988; *Shen and Forsyth*, 1995; *Presnall et al.*, 2002; *McKenzie et al.*, 2005]. A potential temperature of ~1550°C is required for the production of Hawaiian magmas and Gorgona komatiites with 18–19% MgO, and >1600°C for Gorgona picrites with 23% MgO. The excess temperature ΔT_P is the difference between the potential temperature of an oceanic island mantle source and ambient mantle that produced MORB. It is typically about 200–300°C (Figure 5), which is in good agreement with other estimates [i.e., *McKenzie and O'Nions*, 1991; *Watson and McKenzie*, 1991; *Schilling*, 1991; *Herzberg and O'Hara*, 2002; *Putirka*, 2005]. Our excess temperatures displayed in Figure 5 provide important support for thermal anomalies predicted in the mantle plume model. However, ΔT_P is also variable, and Iceland at the present time is only moderately hotter than ambient mantle.

[40] Archean Al-undepleted komatiites with 27–30% MgO had eruptions temperatures of 1550–1600°C (Figure 5), and strong depletions in incompatible trace elements indicate they erupted dry [*Arndt et al.*, 1998]. The potential temperature must have been considerably higher than 1600°C, the liquidus temperature for a magma with 30% MgO, because potential temperatures are always higher than eruption temperatures for the case of adiabatic decompression melting [e.g., *McKenzie and Bickle*, 1988]. These are among the highest eruption temperatures in the terrestrial rock record, possibly exceeded only by Perseverance and Barberton komatiites with parental magmas that have been estimated to contain 33–34% MgO [*Nisbet et al.*, 1993; *Kareem and Byerly*, 2003]. Archean komatiites might have begun to melt at pressures greater than ~10 GPa [*Sproule et al.*, 2002], but at these conditions there are no reliable adiabatic

decompression melting models. Nevertheless, a potential temperature in the 1700–1900°C range appears necessary. This compares with a potential temperature of ~1500–1600°C for Archean ambient mantle, estimated from a secular Earth cooling model of 50–100°C/Ga [*Pollack*, 1997] and our potential temperature for modern ambient mantle (Figure 5). Thus Archean komatiites might have formed in mantle plumes that were ~250°C hotter than Archean ambient mantle, similar to ΔT_P of modern plumes.

6. Analysis of Temperature Uncertainties

[41] The 1-atm olivine liquidus crystallization temperatures of the primary magmas have been calculated using the method of *Beattie* [1993]. This method yields predicted olivine crystallization temperatures that differ from observed temperatures by ±31°C at the 2σ level of confidence. The uncertainty arises from laboratory experiments on a large number of compositions that span the basalt – picrite compositional spectrum. They are also similar to temperatures obtained using the method of *Ford et al.* [1983] and agree to within 13°C of those obtained by MELTS [*Ghiorso and Sack*, 1995; *Asimow et al.*, 2001] for magmas with MgO in the 10–20% range, and within 21°C for magmas with 30% MgO. MELTS yields computed 1 atm olivine liquidus crystallization temperatures that differ from experimental temperatures by ±55°C at the 2σ level of confidence; the uncertainty drops to ±41°C when the database is filtered for analyses with 0–5% Na_2O, compositions that are most appropriate to magma compositions in this study. The agreement in predicted temperature from Beattie and MELTS is therefore extremely good despite fundamental differences in the theoretical approaches to the parameterizations (i.e., thermodynamic versus empirical).

[42] In a more recent study *Putirka* [2005] provides another parameterization of an experimental database consisting of 750 olivine-liquid pairs. However, the *Putirka* [2005] liquidus temperatures are invariably higher because his parameterization includes high-pressure anhydrous experimental data that always have higher olivine liquidus temperatures. For example, *Putirka* [2005] calculates anhydrous liquidus temperatures of 1375 and 1565°C for MORB and Hawaiian liquids having 13 and 19% MgO, respectively, and in equilibrium with olivine having Fo 90.5. Our calculations yield 1301 and 1433°C, lower than *Putirka*'s [2005] by 74°C for MORB and 132°C for Hawaii. The more recent *Putirka et al.* [2006] study provides temperatures that are in better agreement with *Beattie* [1993] and this study.

[43] The mixing of differentiated magmas in a magma chamber with a fresh batch of primitive magmas from the mantle can contribute to another uncertainty. For example, *Rhodes et al.* [1979] described MORB glasses from near the Kane Fracture Zone that display an early history of cotectic crystallization, yet contain olivine as the only phenocryst phase. Calculated parental magma compositions that have undergone this type of mixing will also have elevated FeO contents, and this will propagate to elevated MgO contents and erroneously high temperatures.

[44] Experimental petrology on partially molten peridotite provides information about crystal-liquid equilibrium, which must then be parameterized in order to simulate the fractional melting process described for Figure 1b, often termed a melting model. In all cases it is assumed that melting begins and ends along one adiabatic path, and the primary magmas are formed by the integration of all fractional melts along the vertical streamline. Increasing mantle potential temperature initiates melting at higher pressures, and this produces primary magmas with higher MgO contents in all melting models [*Klein and Langmuir*, 1987; *Niu and Batiza*, 1991; *Langmuir et al.*, 1992; *Kinzler*, 1997; *McKenzie and Bickle*, 1988; *McKenzie and O'Nions*, 1991; *Watson and McKenzie*, 1991; *Herzberg and O'Hara*, 2002; *Asimow et al.*, 2001; *Ghiorso and Sack*, 1995]. All models provide the same T_P for primary magmas with 10–13% MgO, but the variation can be ±50°C for primary magmas with 18–20% MgO relative to the model of *Herzberg and O'Hara* [2002].

7. Analysis of Uncertainties Stemming From Lithologically Heterogeneous Mantle

[45] There is presently no consensus about the rock type that is melting below Hawaii, and most studies usually assume that either peridotite or pyroxenite melt to produce the abundant tholeiites. However, recent work indicates that both peridotite and pyroxenite melt to yield the lavas on Hawaii [*Sobolev et al.*, 2005; *Herzberg*, 2006]. Although basaltic crust can melt at much lower temperatures than peridotite [*Yasuda et al.*, 1994; *Yaxley and Green*, 1998; *Pertermann and Hirschmann*, 2003],

there is a range of pyroxenite source compositions that can have solidus temperatures that are comparable to peridotite [*Kogiso et al.*, 2004; *Herzberg*, 2006]. A detailed analysis is well beyond the scope of this paper. The relationship between temperature and MgO contents of liquids developed in this work is essentially based on olivine-liquid equilibria. While the inverse modeling (i.e., the estimation of parental magma composition and eruption temperature) is valid for any magma that crystallizes olivine phenocrysts at low pressure, the forward component (i.e., derivation of primary magma from parameterization of melting experiments) is only valid for an olivine-bearing residue. Indeed, partial melts of an olivine−free pyroxenite source with compositions near the pyroxene-garnet thermal divide of *O'Hara and Yoder* [1967] can be hotter than melts of a peridotite source even though they are lower in MgO [*Herzberg*, 2006]. A restriction is that there is a broad similarity in Mg # of peridotite and pyroxenite sources [*Kogiso et al.*, 2004]. Source temperatures inferred from the MgO contents of a substantial range of pyroxenite melts can be too low [*Herzberg*, 2006]. For this reason, our estimate of the mantle potential temperature below Hawaii is based on lavas that are identified as having been extracted from a peridotite source [*Herzberg*, 2006].

8. MORB and an Analysis of Alternate Mantle Potential Temperature Models

[46] Understanding the MgO content of primary NMORB magmas is important because it constrains the potential temperature of ambient mantle. Our primary NMORB magmas have 10–13% MgO, in good agreement with many previous estimates [*Presnall and Hoover*, 1987; *McKenzie and Bickle*, 1988; *Niu and Batiza*, 1991; *Kinzler and Grove*, 1992; *Herzberg and O'Hara*, 2002]. However, there is a long history of divergent views that must be resolved because every 1% error in the MgO content of primary NMORB propagates to an error of ~30°C in mantle potential temperature, which is ~1/3 the total range for ambient mantle (Figure 5). For example, in the view of *Green et al.* [2001], primary MORB magmas have 16% MgO, the same as the primary magma for Hawaii, and these melted from mantle at the same potential temperature (i.e., T_P = 1430°C). In contrast, *Langmuir et al.* [1992] concluded that the MgO contents for primary MORB range from 10 to 18%, requiring large temperature variations of ambient mantle below oceanic ridges (i.e., T_P = 1300–1570°C). The mantle plume model is not required by either of these alternate models, which we now examine.

8.1. Model of *Green et al.* [2001]

[47] *Green et al.* [2001] compute primary magma compositions by addition of olivine using algorithms in the software of *Danyushevsky* [2001]. We have reproduced their calculations using this software, in order to examine their method and assumptions in some detail.

8.1.1. Hawaii

[48] We will restrict this analysis of their Hawaii results to their primary magma estimate for Mauna Loa sample ML-1868, and the average of 7 picritic glasses from Kilauea. Mauna Loa sample ML-1868 is an olivine-rich picrite with Fo 91.3 phenocrysts and the whole rock analysis is reported to have 21.48% MgO and 11.37% FeO_T [*Norman and Garcia*, 1999]. The Kilauea glasses contain Fo 90.7 olivine and have 14.72% MgO and FeO_T = 11.24% [*Clague et al.*, 1991]. For the Mauna Loa parental magma, *Green et al.* [2001] obtain 18.4% MgO and we obtain 19–20% MgO. For Kilauea, *Green et al.* [2001] obtain 16.6% MgO and we calculated 18% MgO. The main reason why the MgO contents of *Green et al.* [2001] are slightly lower is because for the same FeO_T, they adopt a slightly lower value for FeO [see also *Putirka*, 2005]. This is due to their assumption that $Fe^{3+}/\Sigma Fe$ = 0.15–0.20 in Hawaiian glasses, which is 0.5 log units more oxidizing than QFM. In contrast, we use $Fe^{3+}/\Sigma Fe$ = 0.06–0.10, as constrained by ferrous iron measurements [*Wright et al.*, 1975; *Rhodes and Vollinger*, 2005].

[49] In summary, our computational methods for individual samples yield similar results for Hawaii, although our MgO contents are higher by about 1–2% absolute because we adopt more reducing conditions. Additionally, there is substantial similarity in our peridotite-source primary magma estimate (18–19% MgO; Figure 3) and our estimated 50°C lowering of magmatic temperature owing to volatile effects (Figure 5). However, *Green et al.* [2001] examined other Hawaiian lavas and calculated an MgO range of 13.5–18.4%. They then decide that the average Hawaiian parental magma contains 16% MgO, and use this as the basis for concluding T_P = 1430°C below Hawaii. Outstanding difficulties are as follows: (1) they do not state how they arrive at this potential temperature (see Figure 5); (2) in the plume model,

primary magmas with the highest MgO contents are expected to form in a hot axis, and those with the lowest MgO will form at the plume periphery. It is the highest MgO content that defines the potential temperature of a plume, this being 18–19% MgO for Hawaii [*Green et al.*, 2001; this work]; and (3) a lithologically heterogeneous source can produce primary magmas with a range of MgO contents at constant temperature.

8.1.2. MORB

[50] We now examine the conclusion of *Green et al.* [2001] that primary MORB magmas can contain 16% MgO, in contrast with our estimate of 10–13%. The difference is significant because it can propagate to T_P for ambient mantle that is too high by 70°C, a range that spans half of the temperature variability of ambient mantle (Figure 5).

[51] *Green et al.* [2001] calculated primary magma compositions using eight MORB glasses with Fo 91.5–92.0 olivines, and these calculations are reproduced in Figure 6. Half of these samples come from a section of the Mid-Atlantic Ridge that was affected by Azores magmatism (enriched MORB samples in Table 2 of *Green et al.* [2001]), and these are not representative of normal MORB [e.g., *Langmuir et al.*, 1992]. Two samples with high FeO contents from Ocean Drilling Prograpm Site 896, east of the both the Galapagos archipelago and the Galapagos Rift, contain olivines with Fo 91.6 [*McNeill and Danyushevsky*, 1996]; these are samples 148-896A-27R-1,15 and 148-896A-3R-1,4 and, although they might have been influenced by the Galapagos plume, we initially consider these as NMORB. Two other samples come from a normal ridge. Sample D20-20, from the Siqueiros transform fault on the East Pacific Rise, contains Fo 91.5 [*Perfit et al.*, 1996], and sample DSDP 3-18, from the southern Mid-Atlantic Ridge, contains olivine phenocrysts with maximum Fo of 89.7 [*Green et al.*, 1979]. Maximum Fo contents in olivines from NMORB are 91.5–91.6.

[52] *Green et al.* [2001] used $Fe^{2+}/\Sigma Fe = 0.93$ for all samples [*Christie et al.*, 1986], a value we will also use. This analysis will be restricted to the same four NMORB samples used by *Green et al.* [2001]. However, for MORB from the Siqueiros Fracture Zone sample, we use sample ALV2384-007B [*Perfit et al.*, 1996], which is similar to but slightly more primitive than sample D20-20 used in the study by *Green et al.* [2001].

[53] All glass samples used by *Green et al.* [2001] are the end products of fractional crystallization. In order to restore the parental magma composition, we need to understand which minerals have crystallized, and the compositions of these minerals. *Green et al.* [2001] assumed that the only crystallizing mineral was olivine in all cases despite the occurrence of phenocrysts of plagioclase and in some cases augite in three of these glasses (DSDP3-18; 148-896A-3R, 27R). They reconstructed their parental magmas by adding olivine only to their glass compositions, and the procedure was stopped when the calculated olivine compositions matched the observed phenocryst olivine compositions, which they assumed to be Fo 91.5–92.1 for the eight MORB glasses. They then assumed that their parental and primary magmas had the same composition. Their procedure yields primary MORB with 13.0–15.5% MgO (Figure 6), some of which are similar to their 16.0% MgO for Hawaii. Therefore they concluded that primary MORB and Hawaii formed by mantle sources that were about equally hot.

[54] It is important to understand how MgO and FeO vary in lavas that crystallize plagioclase and augite in addition to olivine. The fields shown in Figure 6 have been calibrated from experiments [*Grove and Bryan*, 1983; *Yang et al.*, 1996] and the liquid lines of descent for Hawaii, Iceland, and MORB from the Siqueiros fracture zone. For D20-20 and DSDP3-18, the only samples treated by *Green et al.* [2001] that are likely to have crystallized olivine alone, olivine was added incrementally as discussed above. Parental magmas for the remaining 2 samples from the Galapagos Rift were restored by addition of olivine + plagioclase ± augite using PETROLOG software of *Danyushevsky* [2001] until intersection with the multiple saturation boundary shown in Figure 6, followed by addition of olivine alone, using the 1 atm K_D model of *Toplis* [2005].

[55] The first difficulty encountered by *Green et al.* [2001] was that their parental magma for MAR sample DSDP 3-1 was restored by using Fo 91.5 as the target olivine composition, and they obtained 13.2% MgO. In contrast, observed phenocrysts have Fo 89.7 [*Green et al.*, 1979], and this yields 10.4% MgO. For MORB from the Siqueiros Transform (Fo 91.5), we obtain 14% MgO, similar to that obtained by *Green et al.* [1979]. However, for MORB from the Galapagos Rift (Fo 91.6), we calculate 13% MgO whereas *Green et al.* [1979] obtained 15–16% MgO. This difference results

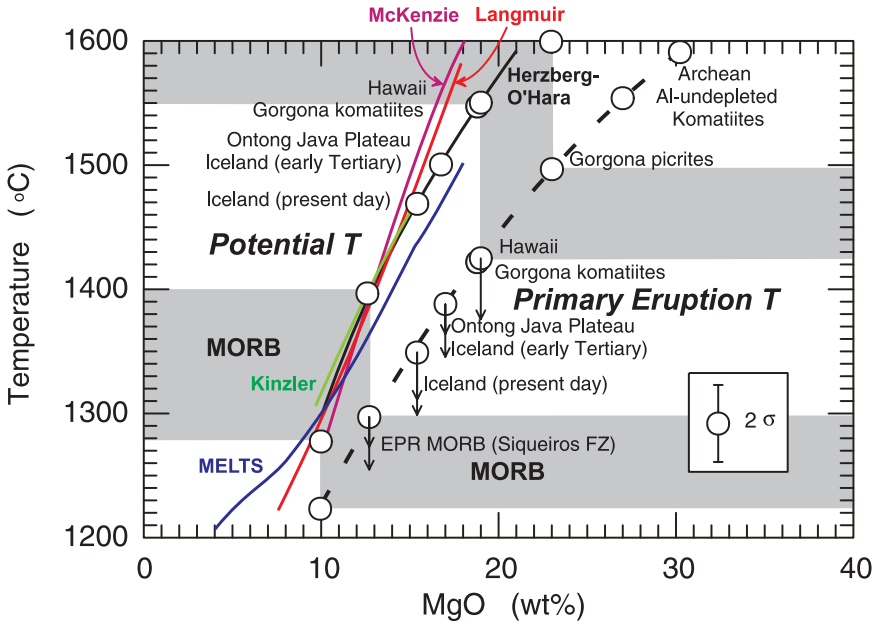

Figure 5. Primary eruption and mantle potential temperatures as a function of the MgO contents of primary magmas. Circles indicate MgO contents of primary magmas from Figure 3. Potential temperature model sources are *Herzberg and O'Hara* [2002], McKenzie [*McKenzie and Bickle*, 1988; *McKenzie and O'Nions*, 1991; *Watson and McKenzie*, 1991], Langmuir [*Klein and Langmuir*, 1987; *Langmuir et al.*, 1992], *Kinzler* [1997], and MELTS [*Ghiorso and Sack*, 1995; *Asimow et al.*, 2001]. Primary eruption temperatures are anhydrous olivine liquidus temperatures at 1 atm calculated for the primary magmas shown in Figure 3 using the method of *Beattie* [1993]; the bracket shows the uncertainty at the 2σ level. The method of Beattie can be simplified to the equation $T(^{\circ}C) = 935 + 33MgO - 0.37MgO^2$ for a wide range of mafic and ultramafic compositions, illustrated by the dashed curve (wt % MgO). Potential temperature can be calculated from $T_P(^{\circ}C) = 1463 + 12.74MgO - 2924/MgO$ [*Herzberg and O'Hara*, 2002]. Arrows display the effects of H_2O content on liquidus temperature (see text). Partial crystallization of primary magmas will yield actual eruption temperatures that are lower than primary eruption temperatures.

from their use of higher FeO contents, and this arises because they added olivine directly to glasses without correcting for crystallization of plagioclase and augite phenocrysts in the lavas.

[56] We now estimate primary magma compositions for the four NMORB samples using the coupled forward inverse method described in section 2.2 above, and these yield 12–13% MgO (Figure 6). These primary magma compositions are somewhat lower in MgO than "parental" magmas computed by olivine addition, an apparent paradox that we resolved above by considering the effects of fractional melting. *Green et al.* [2001] assumed that parental magmas calculated by olivine addition are always the same as primary magmas produced by batch melting. This interpretation is not likely because the implied melt fractions would be too high (Figure 1b and Appendix A).

[57] MORB from the Siqueiros Transform with ~7.0% FeO define the most primitive end-member of a wide range of compositions of MORB from the East Pacific Rise. The primary magmas have 12–13% MgO, representative of MORB from the fastest spreading center. Shown also are MORB from the Cayman Rise, notable in being samples from the slowest spreading center and having the lowest FeO contents [*Langmuir et al.*, 1992]. Cayman Rise MORB are also the products of extensive fractional crystallization [*Elthon et al.*, 1995; *Langmuir et al.*, 1992], and restoration to olivine with Fo ~90 will yield a primary magma with MgO ~10% (Figure 6). MORB from the Mid-Atlantic Ridge exhibits a considerable range of FeO at 8% MgO, and a clear understanding of this variability is compromised by the influence of Azores magmatism. Similarly, high MgO contents derived from Galapagos Rift glasses in both this study and that of *Green et al.* [2001] are possibly an artifact of interaction with the Galapagos plume. Although Galapagos Rift glasses appear to be NMORB, the Galapagos plume is heterogeneous, with both enriched and depleted geochemical properties [*White et al.*, 1993; *Werner et al.*, 2003]. The

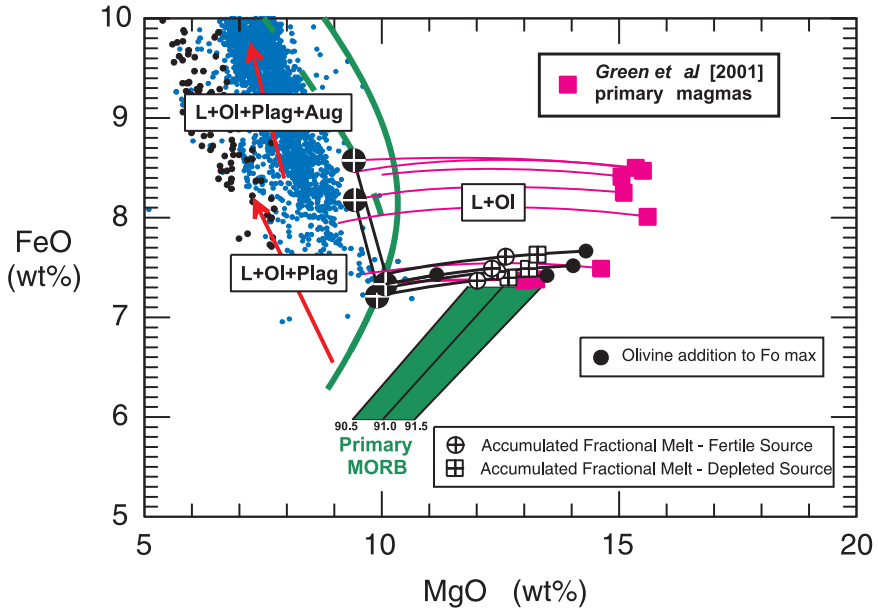

Figure 6. FeO and MgO contents of primary magmas for oceanic ridges estimated by *Green et al.* [2001] compared to this work. Both studies use $Fe^{2+}/\Sigma Fe = 0.93$ [*Christie et al.*, 1986]. Magenta lines terminating in circles and squares indicate eight MORB glass compositions and their primary magmas estimated by olivine addition, respectively [*Green et al.*, 2001]. Of these eight glasses, four are normal MORB which we reexamine in our model: black circles with white crosses indicate four NMORB glasses; black circles indicate "parental" NMORB magmas computed by olivine addition; white circles and squares with black crosses indicate accumulated fractional melt compositions of fertile and depleted peridotite that are candidate primary NMORB compositions. Solid green curve separates liquids that crystallized olivine only on the MgO-rich side from liquids that crystallize olivine + plagioclase ± augite to the MgO-poor side; these are valid for MORB, Iceland, and hot spot-influenced MORB from Reykjanes Ridge, Galapagos Ridge, and the FAMOUS area of MAR influenced by the Azores. Dashed green curve is similar but is valid for more SiO_2-rich compositions such as Hawaii. Red arrows depict general FeO-MgO fractionation vectors. All MORB glasses are from the Petrological Database of the Ocean Floor (PETDB) (http://www.petdb.org). Blue dots indicate MORB from the East Pacific Rise. Black dots indicate MORB from the Cayman Rise. Green area indicates our preferred primary MORB magmas that would crystallize olivine with the compositions shown at the surface.

range of MgO for primary normal MORB magmas is 10–13%.

8.2. Model of *Langmuir et al.* [1992]

[58] There appears to be considerable confusion in the scientific community about the interpretation of results given by *Langmuir et al.* [1992], so we will clarify our understanding of this pioneering study. *Langmuir et al.* [1992], in our view, correctly identify the meaning of Na8, Fe8, and axial depth, the correlations among these parameters, and the central role of potential temperature variations among ridge segments. The 270°C variation in ambient mantle potential temperature below ridges in the model of *Langmuir et al.* [1992] arises from two sources: (1) their primary magmas that have MgO contents in the 10–18% range and (2) their use of a model anhydrous solidus that is linear in T-P space. We will focus on their petrological modeling, which is summarized in Figures 15c and 53 of Langmuir et al. In these diagrams they show MORB from normal ridges and those from ridges "influenced by" or "immediately adjacent to" hot spots. However, the handling of Iceland is ambiguous. The caption to Figure 15 of *Langmuir et al.* [1992] notes that Iceland and adjacent ridges are coincident with the normal MORB array. In Figure 53 of Langmuir et al. the caption states that only normal ridge segments are shown, yet visual inspection of the two figures shows that the highest $Fe_{8.0}$ point on Figure 53 is for Iceland. In short, the conclusion of *Langmuir et al.* [1992] should have been, apparently, that ridges removed from the influence of all hotpots except Iceland show a 270°C temperature range. The high end of the array is anchored by Iceland, and the methods used show a continuously populated normal ridge trend

extending up to Iceland with no gap. Langmuir et al.'s Figure 53, for which they draw their conclusions, shows Fe8.0 = 7.6 to 11.9 for normal MORB, and from equation (29) of Langmuir et al., Po = 12 to 38 kbar, where Po is the initial melting pressure. Reference to Langmuir et al.'s Figure 48 shows that their primary normal MORB has 10–18% MgO. Application of Po = 12 to 38 kbar to their Figure 57 yields a potential temperature range of 1300 to 1570°C, a difference of 270°C, which we show also in Figure 5. *Langmuir et al.* [1992] derive a temperature for range for normal MORB as large as our range for both normal MORB and Hawaii.

[59] We now examine the petrological basis for the large range of T_P in the *Langmuir et al.* [1992] model. Many of the plots of *Langmuir et al.* [1992] contrast the geochemistry of different lava series by normalizing their variability to 8.0% MgO (i.e., Na_8, Fe_8; where Fe refers to total iron as FeO_T). However, it is often clearer to make direct plots of MgO versus Na_2O and FeO_T, as shown in Figure 7 for a wide range of lavas, and to compare these to the *Langmuir et al.* [1992] model primary magmas generated by accumulated fractional melting. Of all ridge lavas on Earth, those from the Cayman Rise have the highest Na_2O and lowest FeO_T, and lavas from the Reykjanes Ridge have the lowest Na_2O and highest FeO_T. Lavas from all other ridges plot between these extremes, as demonstrated by those from the East Pacific Rise (Figure 7).

[60] Lavas from the Reykjanes Peninsula and the Theistareykir segment of the northern volcanic zone in northeast Iceland [*Slater et al.*, 2001; *Maclennan et al.*, 2003] have a major element geochemistry and abundant olivine-rich picrites that are essentially identical. Lavas from the Herdubreid region, farther to the south and closer to the central part of Iceland, are not as olivine-rich but nevertheless display Na_2O and FeO_T contents [*Maclennan et al.*, 2001] at around 10% MgO similar to Reykjanes and Theistareykir. It is further noted that lavas from Iceland and the Reykjanes Ridge have trace element and isotopic characteristics that are distinct from normal MORB [*Kempton et al.*, 2000; *Thirlwall et al.*, 2004]. Therefore there is reason to expect differences in major element geochemistry for the sources of normal MORB and Reykjanes Ridge MORB and it is suspect to anchor normal MORB with Reykjanes MORB.

[61] The *Langmuir et al.* [1992] model in Figure 7 indicates initial melting pressures are between 1.2 and 2.0 GPa for Cayman Rise and 2.0–3.0 GPa for East Pacific Rise. These pressure ranges are consistently obtained using either Na_2O or FeO_T. It is our interpretation that this aspect of the *Langmuir et al.* [1992] model provides a good description of the entire range for MORB on Earth, which corresponds to a T_P range of 1300–1400°C as indicated also by our work.

[62] Problems, however, begin to emerge when drawing pressure information from the *Langmuir et al.* [1992] model for Reykjanes MORB and Iceland. Pressures of >3.0 GPa are inferred from Na_2O for nearly all Iceland and Reykjanes samples (Figure 7a), but pressures of <3.0 GPa are required from FeO_T in many of the same samples (Figure 7b). These contradictory results reveal problems in the forward *Langmuir et al.* [1992] model for lavas with high FeO_T and low Na_2O.

[63] A complete petrological resolution to these problems is beyond the scope of this paper. However, in Figure 8 we offer an alternate MgO-FeO_T diagram, based on the peridotite melting models of *Herzberg and O'Hara* [2002] and *Herzberg* [2004a]. It is noted that this diagram will be strictly applicable to melts that form from a peridotite source. Furthermore, there is some indication that Reykjanes lavas were derived from a lithologically heterogeneous source consisting of both peridotite and clinopyroxenite. Although this well beyond the scope of the present study, lavas from both sources have essentially identical MgO-FeO systematics, indicating that Figure 8 remains a useful diagram.

[64] There is fairly good agreement with the *Langmuir et al.* [1992] model for lavas low in FeO_T, and all MORB can be reasonably described by initial melting in the 2.0–3.0 GPa range, yielding primary magmas with ~10–13% MgO formed in the T_P range of 1300–1400°C. On this point, we agree with *Langmuir et al.* [1992] that the average MgO content for normal MORB is ~12%. We also agree with *Langmuir et al.* [1992] that lavas from the Reykjanes Ridge and Iceland are hotter than normal MORB, a conclusion reached also by *Putirka* [2005]. However, we obtain primary magmas with MgO in the 14–16% range instead of 18% as in the work by *Langmuir et al.* [1992] and initial melting in the 3.0–3.6 GPa range (Figure 8). This revised pressure range is considerably higher than ~2.5 GPa inferred in the *Langmuir et al.* [1992] model for FeO_T (Figure 7b). Our preferred potential temperature is about 1460°C, in good agreement with 1480°C recommended by *Slater et al.* [2001] but significantly lower than 1570°C in

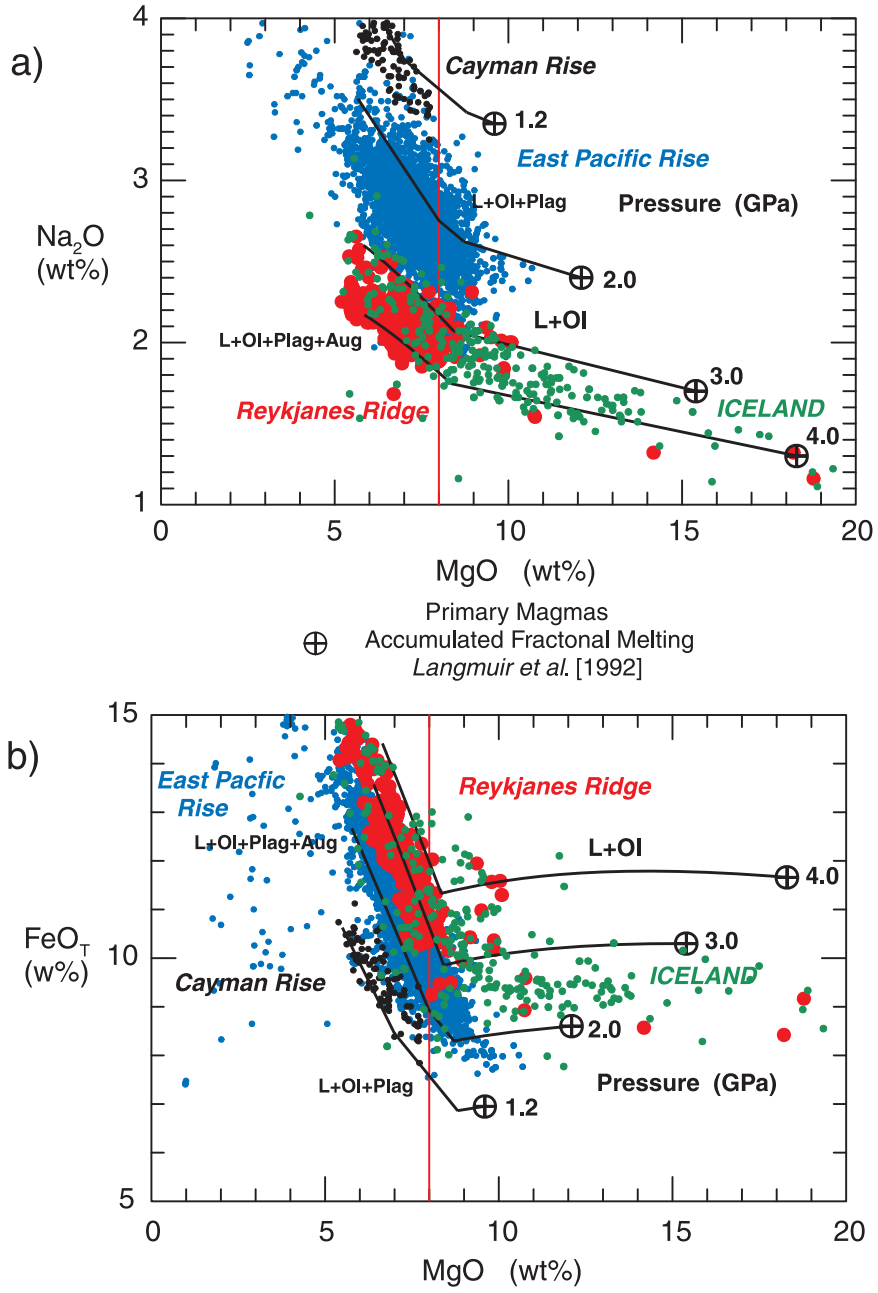

Figure 7. Forward melting and crystallization model of *Langmuir et al.* [1992] compared to glasses and whole rocks from the Cayman Rise (PETDB), East Pacific Rise (PETDB), Reykjanes Ridge (PETDB), and Theistareykir on Iceland [*Slater et al.*, 2001; *Maclennan et al.*, 2003]. Trends for the fractionation of olivine [L + Ol], olivine + plagioclase [L + Ol + Plag], and olivine + plagioclase + augite [L + Ol + Plag + Aug] were calculated using methods of *Langmuir et al.* [1992]. The inflexions that occur from [L + Ol] to [L + Ol + Plag] for lava compositions rich in FeO_T and poor in Na_2O were placed at 8.5% MgO (C. H. Langmuir, personal communication, 1998, to P. D. Asimow) which is too low, as shown in Figure 6.

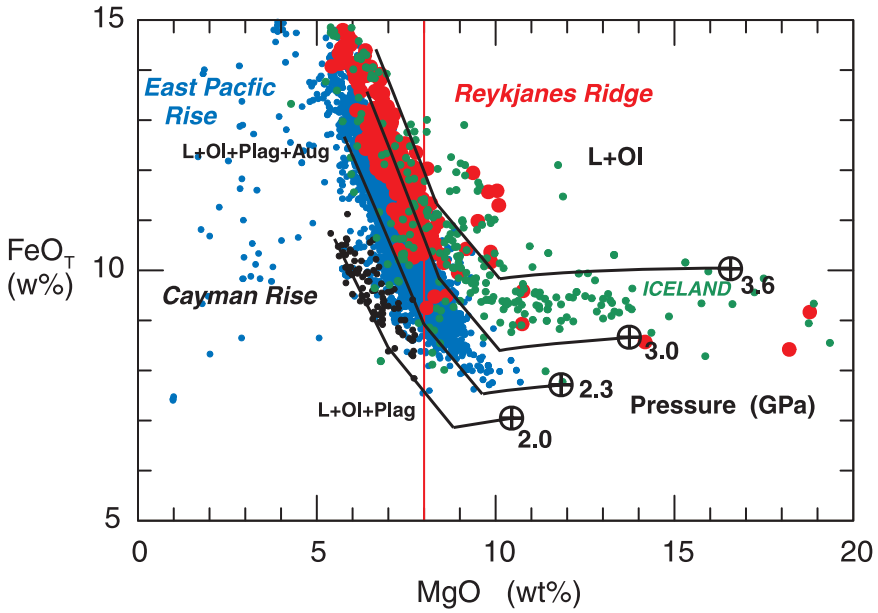

Figure 8. A revised forward melting and crystallization model compared to glasses and whole rocks from the Cayman Rise, East Pacific Rise, Reykjanes Ridge, and Theistareykir from the north volcanic zone in Iceland. Data sources are given in Figure 7. For simplicity, we assume the following crystallization sequence at the surface: L + Ol → L + Ol + Plag → L + Ol + Plag + Aug.

Langmuir et al. [1992]. We emphasize, however, that these interpretations apply strictly to Iceland, not to normal MORB, and they should not be used as a high T_P anchor for ambient mantle. Our preferred T_P range for ambient mantle is 1280–1400°C (Figure 5). Thus it is a small T_P variation of only ~120°C that produces a large range in Na8 and Fe8 observed in normal MORB.

9. Mantle Temperatures and the Plume Hypothesis

[65] *Wilson* [1963] defined hot spots as thermally anomalous volcanic areas and *Morgan* [1971] related them to deep mantle plumes, which he suggested are narrow vertical conduits carrying hot deep mantle material toward the surface. Although plume buoyancy might, in some cases, be attributed to compositional differences, more commonly a plume is assumed to rise because its temperature is greater than that of ambient mantle. Plumes are thought to originate at a thermal boundary layer, which might be the core-mantle boundary [*Loper and Stacey*, 1983]. However, not all plumes need be rooted to a thermal boundary layer [*Davies and Bunge*, 2006]. High excess temperatures at the core-mantle boundary can be reduced to 250°C at the surface [*Bunge*, 2005]. Some plumes might flow throughout the mantle, and others might be confined to the upper mantle [*Montelli et al.*, 2004]. The simple mushroom-like structure for purely thermal plumes [*Campbell and Griffiths*, 1990] can transform to complex structures and flow properties owing to compositional contributions to buoyancy [*Lin and van Keken*, 2005; *Farnetani and Samuel*, 2005]. Plumes may have high or low H_2O contents [*Dixon et al.*, 2002; *Arndt et al.*, 1997], and they may lower seismic wave velocities because they are either hot or wet [*Karato*, 2004]. They can be geochemically variable, with depleted and enriched properties. Also, some plumes might be hotter than others, as we showed in this paper (Figure 5). Although plumes might exhibit substantial diversity, they all have in common the intrusion of anomalous mantle into ambient mantle.

[66] Thermal anomalies are thought to occur in some plume conduits ~10^2 km across, close to the limits to seismological resolution of deep mantle structure [*Allen et al.*, 1999; *Foulger et al.*, 2001; *Montelli et al.*, 2004]. In contrast, thermal variations associated with ambient mantle occur on a scale and wavelength that is about an order of magnitude greater, ~10^3 km. Therefore some plumes are predicted to have the properties of point sources of heat and magmatism, forming *Wilson*'s [1963] "hot spots." The broad seismologically slow regions under Africa and the Pacific,

called superplumes, might actually be clusters of smaller plumes [*Schubert et al.*, 2004] of uncertain temperature and H_2O content.

[67] Our work shows that ambient mantle temperatures at normal oceanic ridges are 1280–1400°C (ΔT_P = 120°C), similar to other estimates [*Shen and Forsyth*, 1995; *Presnall et al.*, 2002]. This contrasts with 1300–1570°C (ΔT_P = 270°C) estimated by *Langmuir et al.* [1992] and 1400–1600°C (ΔT_P = 200°C) by *Anderson* [2000]. The mantle below hot ridges in the models of Langmuir and Anderson is as hot as our mantle below Hawaii.

[68] Our calculated potential temperature below Hawaii is ~1550°C (Figure 5), in good agreement with other estimates [*Watson and McKenzie*, 1991; *McKenzie and O'Nions*, 1991; *Sobolev et al.*, 2005]. Its association with a slow seismological anomaly [*Montelli et al.*, 2004] is consistent with the expectations of a plume. An alternative to the plume model is a broad region of hot ambient mantle below the central Pacific plate [*Anderson*, 2000]. This is not consistent with significant source temperature variations below Hawaii [*Sobolev et al.*, 2005; *Herzberg*, 2006]. Anderson's model would predict widespread melting over a large region, and yield many hot spots with the petrological properties of Hawaii. This prediction is not supported by the petrology of basalts from the North Arch region 600 kilometers north of Hawaii [*Dixon et al.*, 1997] and basalts from the Line Islands about 1200 kilometers southwest of Hawaii [*Davis et al.*, 2002]. These peripheral volcanic fields are distinguished from the shield building lavas of Hawaii in being exclusively alkalic basalts formed by low degrees of melting at cooler mantle source temperatures. Hawaii is a point source of heat and magmatism, a hot spot, consistent with *Morgan*'s [1971] proposal that it is forming above a deep mantle plume.

[69] Our calculated potential temperature below present-day Iceland is about 1460°C (Figure 5), in good agreement with other estimates [*Slater et al.*, 2001]. However, there is evidence that it was hotter in the early Tertiary [*Saunders et al.*, 1997; *Herzberg and O'Hara*, 2002] as inferred from picrites from Baffin Island and West Greenland. These crystallized from primary magmas with 17–18% MgO, higher than present-day Iceland but lower than Hawaii (Figure 3). In the context of the plume model, these magmas are associated with an earlier stage of the plume that continues to drive Iceland magmatism. Eruptions occurred over a much larger area of the North Atlantic Igneous Province when the plume head first impinged on, and spread laterally, below the base of the lithosphere [*White and McKenzie*, 1989; *Saunders et al.*, 1997].

[70] The potential temperatures needed to produce the Gorgona picrites were in excess of 1600°C, hotter than any other Phanerozoic occurrence. Melting must have started deep and ended shallow in order to generate the high melt fractions necessary to explain Fo 93.6 olivines and extreme depletions in trace elements. It is difficult to imagine how this could have happened by passive upwelling beneath a spreading center.

[71] High MgO contents and eruption temperatures of Archean komatiites shown in Figure 5 provide additional support for the plume model [*Cawthorn*, 1975; *Fyfe*, 1978; *Jarvis and Campbell*, 1983; *Arndt*, 1986b; *Nisbet et al.*, 1993; *Sproule et al.*, 2002; *Herzberg*, 2004a]. The more common basaltic rocks in Archean greenstone belts might be Archean equivalents of modern MORB if they melted from ambient mantle [*Herzberg*, 2004a].

[72] In summary, there is an abundance of petrological evidence for high eruptive temperatures required in some hot plume models. However, the diversity of large igneous provinces is acknowledged, and the plume model may not be appropriate in all cases [*Saunders*, 2005]. We encourage the exploration of alternate models.

10. Conclusions

[73] Magmas that make crust at oceanic ridges, islands, and plateaus provide a geochemical record of the thermal state of the mantle where they form. However, extracting this thermal information is often based on model calculations that can have large uncertainties and questionable assumptions. This has led to models that are both supportive and in conflict with the mantle plume hypothesis. A critical evaluation is made of these models, and we reveal petrological complexities that are a significant source of errors. We reexamine both parental and primary magma compositions below oceanic ridges, and evaluate the thermal properties of their sources. Parental magma compositions are calculated using olivine phenocrysts with maximum forsterite contents observed in lava flows. These are generally in good agreement with primary magma compositions calculated using the mass balance method of *Herzberg and O'Hara* [2002], and differences reflect the well-known effects of

fractional crystallization. Differences can also arise when Fo-rich olivines from advanced stage fractional melts are confused with those that crystallize from accumulated fractional melts.

[74] Our work favors uniformly low temperatures for ambient mantle below ridges, with localized 200–300°C anomalies associated with some mantle plumes. Small variations in mantle source temperature propagate to large variations in major element geochemistry. More specifically, the following conclusions are drawn. Primary magmas for normal present-day mid-ocean ridges contain 10–13% MgO and are forming from ambient mantle with potential temperatures of 1280–1400°C. In contrast, parental and primary magmas for some Hawaiian lavas contain 18–19% MgO, and require potential temperatures of ~1550°C. Hawaii is a hot spot as there is no evidence that it is part of a broad region of hot ambient mantle. Below Iceland the mantle is cooler than Hawaii, though warmer than any other spreading center, and was hotter during the early Tertiary. Cretaceous picrites from Gorgona contained 23% MgO, crystallized olivine with Fo 93.6, and formed at potential temperatures of 1600°C, hotter than any other Phanerozoic occurrence.

[75] The plume model will not provide a suitable explanation for the origin of every seamount and large igneous province on Earth. However, we conclude that there is an abundance of petrological evidence from volcanoes of all ages for the high eruptive temperatures required by hot mantle plumes.

Appendix A: A Mass Balance Method for Calculating Primary Magma Composition

A1. A Tutorial

[76] In this tutorial, we will show how a primary magma composition can be calculated by using the Ontong Java Plateau (i.e., OJP) as an example. This is offered as a practical supplement to theoretical descriptions given in the text of this paper and elsewhere [*Herzberg and O'Hara*, 2002; *Herzberg*, 2004c]. A step-by-step example is given in Table A1, and results are shown in Figure A1.

[77] Before we begin, let us take an overview of the problem. Imagine a fertile peridotite source that undergoes fractional melting, and all the melt droplets collect and mix to produce an aggregate primary magma. The primary magma contains 17% MgO, and the total melt fraction with respect to the initial source mass is 0.27. Next, the aggregate primary magma enters a crustal magma chamber where it transforms to a derivative melt with ~10% MgO by crystallizing olivine. The derivative melt continues to crystallize of olivine, but is joined by augite and plagioclase in the crustal magma chamber. Aliquots of these derivative melts erupt to the surface and solidify as the red circles in Figure A1, but some may undergo further crystallization of olivine, augite, and plagioclase at the surface. The problem is, how do we reconstruct the primary magma with 17% MgO from the lavas represented as red circles? How do we go back? We begin with the "inverse" component, which is simply the calculation of an array of potential primary magmas by addition of olivine to a selected lava composition. Of the OJP lava compositions reported by *Fitton and Godard* [2004] and shown in Figure A1, sample 1187-8 was chosen for this calculation. It is representative of a set of lavas containing only olivine phenocrysts, and there is no indication from depletions in CaO and Al_2O_3 and enrichments in FeO that it had experience augite or plagioclase fractionation (Figure A1). We need to have some idea of how much of the total iron in 1187-8 is FeO, and have assumed it to be 0.90 [*Herzberg*, 2004c], yielding 1.1% Fe2O3 and 8.9% FeO (Table A1). There is some indication that the calculated FeO content is too high by about 0.1%, which is small and discussed further below.

[78] Olivine is now added to 1187-8 in 1 wt % increments using $K_D = (FeO/MgO)^{ol}/(FeO/MgO)^{L}$ from the model of *Toplis* [2005] at 1 atm. K_D ranges from 0.312 to 0.305 as the MgO content of the liquid goes up, in good agreement with the commonly used models of *Ford et al.* [1983] and *Roeder and Emslie* [1970]. The array of liquid compositions calculated for 1 to 30% olivine addition is given in Table A1, as is the Fo content of olivine in equilibrium with each liquid. These are also shown in Figure A1 together with 5% incremental additions of olivine for clarity. The inverse model is now complete.

[79] When a primary magma forms by melting a peridotite source, it will fractionate only olivine as it rises to the surface [*O'Hara*, 1968]. Although some clinopyroxene fractionation can also occur within the lithospheric mantle [*Albarède et al.*, 1997], it is safe to assume it is not important unless its effects can be clearly demonstrated. Therefore

Table A1. Tutorial Demonstrating the Calculation of the Primary Magma Composition for Lavas From the Ontong Java Plateau

Sample	Percent OL Addition	SiO_2	TiO_2	Al_2O_3	Cr_2O_3	Fe_2O_3	FeO	MnO	MgO	CaO	Na_2O	K_2O	NiO	P_2O_5	Mg # Ol	K_D	F MgO - FeO	F MgO-SiO_2	F Projection
1187-8	0	49.69	0.75	15.01	0.075	1.1	8.9	0.17	9.98	12.51	1.66	0.091	0.025	0.061	86.5	0.312	no solution	0.02	0.18
	1	49.6	0.75	14.9	0.075	1.1	8.9	0.17	10.3	12.4	1.64	0.09	0.028	0.06	86.9	0.312	no solution	0.05	0.19
	2	49.5	0.74	14.7	0.074	1.1	8.9	0.17	10.7	12.3	1.63	0.089	0.03	0.06	87.2	0.312	no solution	0.09	0.20
	3	49.4	0.73	14.6	0.074	1.1	9.0	0.17	11.1	12.2	1.61	0.088	0.033	0.059	87.6	0.312	no solution	0.11	0.21
	4	49.3	0.72	14.4	0.074	1.1	9.0	0.17	11.4	12.0	1.6	0.087	0.036	0.059	87.9	0.312	no solution	0.13	0.21
	5	49.2	0.72	14.3	0.073	1.0	9.0	0.17	11.8	11.9	1.58	0.087	0.039	0.058	88.2	0.312	no solution	0.15	0.22
	6	49.1	0.71	14.2	0.073	1.0	9.1	0.17	12.1	11.8	1.56	0.086	0.042	0.057	88.4	0.312	no solution	0.17	0.22
	7	49.1	0.7	14.0	0.072	1.0	9.1	0.17	12.5	11.7	1.55	0.085	0.046	0.057	88.7	0.311	no solution	0.19	0.23
	8	49.0	0.7	13.9	0.072	1.0	9.1	0.17	12.8	11.6	1.53	0.084	0.049	0.056	89.0	0.311	no solution	0.21	0.23
	9	48.9	0.69	13.7	0.072	1.0	9.1	0.17	13.2	11.5	1.52	0.083	0.053	0.056	89.2	0.311	no solution	0.21	0.24
	10	48.8	0.68	13.6	0.071	1.0	9.1	0.17	13.5	11.4	1.5	0.082	0.057	0.055	89.5	0.311	no solution	0.22	0.24
	11	48.7	0.68	13.5	0.071	1.0	9.1	0.17	13.9	11.3	1.49	0.082	0.061	0.055	89.7	0.311	no solution	0.22	0.25
	12	48.6	0.67	13.3	0.070	1.0	9.1	0.17	14.2	11.1	1.47	0.081	0.065	0.054	89.9	0.311	no solution	0.23	0.25
	13	48.6	0.66	13.2	0.070	1.0	9.1	0.17	14.5	11.0	1.46	0.08	0.069	0.054	90.1	0.310	0.01	0.23	0.25
	14	48.5	0.66	13.1	0.070	1.0	9.1	0.17	14.9	10.9	1.44	0.079	0.073	0.053	90.3	0.310	0.03	0.23	0.26
	15	48.4	0.65	13.0	0.069	0.9	9.1	0.17	15.2	10.8	1.43	0.078	0.077	0.053	90.5	0.310	0.07	0.24	0.26
	16	48.3	0.65	12.8	0.069	0.9	9.1	0.17	15.5	10.7	1.42	0.078	0.081	0.052	90.7	0.310	0.10	0.24	0.26
	17	48.3	0.64	12.7	0.068	0.9	9.1	0.17	15.9	10.6	1.4	0.077	0.086	0.052	90.9	0.309	0.15	0.25	0.26
	18	48.2	0.63	12.6	0.068	0.9	9.1	0.17	16.2	10.5	1.39	0.076	0.09	0.051	91.1	0.309	0.21	0.26	0.27
	19	48.1	0.63	12.5	0.068	0.9	9.1	0.17	16.5	10.4	1.37	0.075	0.095	0.05	91.3	0.309	0.25	0.26	0.27
Primary	19.5	48.1	0.63	12.4	0.070	0.9	9.1	0.17	16.7	10.4	1.37	0.075	0.1	0.05	91.3	0.309	0.27	0.27	0.27
	20	48.0	0.62	12.3	0.067	0.9	9.1	0.17	16.9	10.3	1.36	0.075	0.1	0.05	91.4	0.309	0.30	0.27	0.27
	21	48.0	0.62	12.2	0.067	0.9	9.1	0.17	17.2	10.2	1.35	0.074	0.104	0.05	91.6	0.308	0.32	0.28	0.28
	22	47.9	0.61	12.1	0.066	0.9	9.1	0.17	17.5	10.1	1.33	0.073	0.109	0.049	91.7	0.308	0.35	0.28	0.28
	23	47.8	0.6	12.0	0.066	0.9	9.1	0.17	17.8	10.0	1.32	0.072	0.114	0.049	91.9	0.308	no solution	0.29	0.28
	24	47.8	0.6	11.9	0.066	0.9	9.1	0.17	18.2	9.9	1.31	0.072	0.119	0.048	92.0	0.307	no solution	0.29	0.28
	25	47.7	0.59	11.7	0.065	0.9	9.1	0.16	18.5	9.8	1.29	0.071	0.124	0.048	92.2	0.307	no solution	0.30	0.29
	26	47.6	0.59	11.6	0.065	0.8	9.1	0.16	18.8	9.7	1.28	0.070	0.129	0.047	92.3	0.306	no solution	0.30	0.29
	27	47.6	0.58	11.5	0.064	0.8	9.0	0.16	19.1	9.6	1.27	0.070	0.134	0.047	92.5	0.306	no solution	0.31	0.29
	28	47.5	0.58	11.4	0.064	0.8	9.0	0.16	19.4	9.5	1.26	0.069	0.139	0.046	92.6	0.306	no solution	0.31	0.30
	29	47.4	0.57	11.3	0.064	0.8	9.0	0.16	19.7	9.5	1.24	0.068	0.144	0.046	92.7	0.305	no solution	0.32	0.30
	30	47.4	0.56	11.2	0.063	0.8	9.0	0.16	20.0	9.4	1.23	0.068	0.149	0.045	92.9	0.305	no solution	0.32	0.30
KR-4003		44.9	0.16	4.26	0.41		8.02	0.13	38.12	3.45	0.22	0.09	0.24						
Depleted mantle		44.53	0.04	2.36	0.41	0.2	8.07	0.14	41.8	2.14	0.05	0.02	0.24						

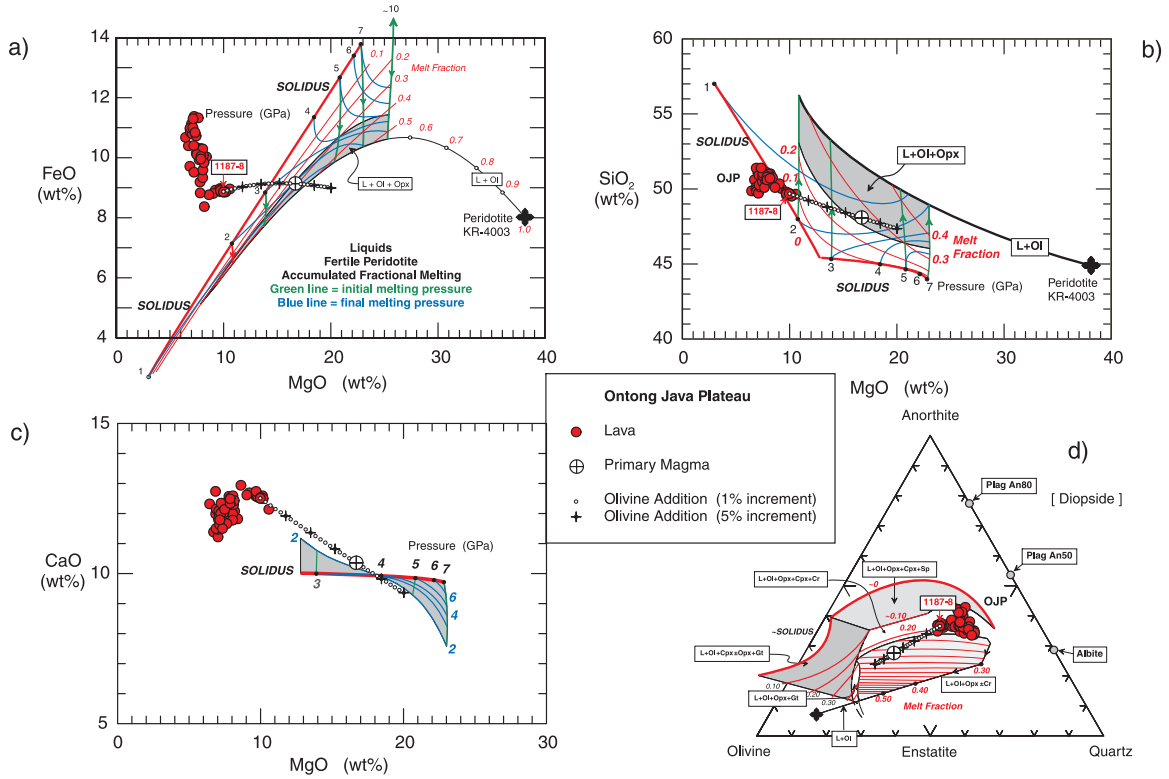

Figure A1. A tutorial that illustrates how compositions of lavas from the Ontong Java Plateau [*Fitton and Godard*, 2004] can be formed by accumulated fractional melting of fertile peridotite KR-4003. Forward model component representing all possible partial melt compositions: thick red lines indicate liquid compositions on the solidus; thin red lines indicate melt fractions with respect to initial source mass of KR-4003; green line with arrows indicates array of accumulated fractional melt compositions that form during decompression at the pressures indicated for initial melting; blue line indicates final melting pressure. Inverse model component: array of small dots indicates liquid compositions produced by adding olivine to lava 1187-8, indicated at 1% and 5% increments; these are also listed in Table A1. Cross in white circle indicates primary magma composition formed by 0.27 mass fractions of melting, a composition that is unique to both inverse and forward models. Figures A1a, A1b, and A1c examine the problem with different oxide components [*Herzberg and O'Hara*, 2002; *Herzberg*, 2004a]. Figure A1d is a projection of liquid compositions (mol %) of fertile mantle peridotite from diopside (CMS_2) and $Na_2O{\bullet}Si_3O_6$ and $K_2O{\bullet}Si_3O_6$ into the plane olivine-anorthite-silica [*Herzberg and O'Hara*, 2002]; projected liquids on the solidus are approximate. Method for calculating a projected composition is given in the caption to Figure 2.

the primary magma for OJP is represented by one of the 30 possible liquid compositions on the olivine-addition arrays shown in Figure A1. But which one?

[80] In order to proceed, we need to know the mineralogy and composition of the source lithology, and the compositions of all partial melts that might be derived from it. This is called the forward model component. Geochemical arguments suggest that the OJP source is similar to a primitive mantle composition that had lost about 1% melt [*Fitton and Godard*, 2004; *Tejada et al.*, 2004]. Extraction of this small amount of melt from *McDonough and Sun* [1995] pyrolite yields a peridotite very similar in composition to KR-4003 [*Herzberg*, 2004c]. This is a very desirable result because there exists high quality melting experiments on KR-4003 [*Walter*, 1998]. Furthermore, these melting experiments have provided the foundation for understanding the compositions of partial melts of KR-4003 that are produced by both batch and accumulated fractional melting [*Herzberg and O'Hara*, 2002; *Herzberg*, 2004a, 2006]. Results for accumulated fractional melting of KR-4003 show that primary magmas of KR-4003 can have a wide range of contents of MgO, FeO, CaO, and SiO_2, depending on initial and final melting pressures and melt fraction as shown in Figure A1. However, which among the range of MgO contents is appropriate for the OJP primary magma?

[81] Our primary magma composition must be common to both inverse and forward model compositions. How is it possible to obtain a unique solution among the 30 possibilities in the inverse model and the infinite number of possibilities in the forward model? We make use of the requirement that the primary magma must form by a very specific mass fraction of melting (i.e., F). The possibilities, shown in Figure A1 and given in Table A1, can then be constrained by asking the basic question: what mass fraction of melting is needed to produce each of the 30 liquids produced by olivine addition in the inverse component? Of the 30 possible liquids listed in Table A1, we comment on five specific cases in order to demonstrate the method. All melt fractions shown in Figure A1 have been provided by *Herzberg and O'Hara* [2002] and *Herzberg* [2004a].

[82] Case 1 is lava 1187-8 (9.98% MgO): F in MgO-FeO space has no solution (Figure A1a). F = 0.02 in MgO-SiO_2 space (Figure A1b). F = 0.18 in projection space (Figure A1d). Composition 1187-8 cannot be a primary magma because there is no agreement among melt fractions. In particular, the MgO content is too low to be a partial melt of fertile peridotite, and there is no solution for the melt fraction in MgO-FeO space. In MgO-SiO_2 space, the melt fraction can be inferred to be 0.02 by visual inspection, a solution that has no significance because it disagrees with F in projection space and the lack of solution in MgO-FeO space. Similarly, F = 0.18 in projection space by visual inspection (Figure A1d), a solution that has no significance because it disagrees with F in projection space and the lack of solution in MgO-FeO space. Within MgO-CaO space, melt fractions have similar compositions [*Herzberg*, 2006], and therefore they are not useful in constraining the problem. All primary magmas of fertile peridotite contain about 10% CaO, an amount that does not vary significantly over a wide range of melting conditions (Figure A1c).

[83] Case 2 is 1187-8 + 5% olivine (12% MgO): F in MgO-FeO space has no solution (Figure A1a). F = 0.15 in MgO-SiO_2 space (Figure A1b). F = 0.22 in projection space (Figure A1d). Composition 1187-8 + 5% olivine cannot be a primary magma because there is no agreement among melt fractions. As above, the MgO content is too low to be a partial melt of fertile peridotite, and there is no solution for the melt fraction in MgO-FeO space.

[84] Case 3 is 1187-8 + 15% olivine (15% MgO): F = 0.07 in MgO-FeO (Figure A1a). F = 0.24 in MgO-SiO_2 space (Figure A1b). F = 0.26 in projection space (Figure A1d). Composition 1187-8 + 15% olivine cannot be a primary magma because there is no agreement among melt fractions.

[85] Case 4 is 1187-8 + 19.5% olivine (17% MgO): F = 0.27 in MgO-FeO (Figure A1a). F = 0.27 in MgO-SiO_2 space (Figure A1b). F = 0.27 in projection space (Figure A1d). Composition 1187-8 + 19.5% olivine is the calculated primary magma composition for KR-3004s because there is agreement that the melt fraction is 0.27 in all cases. It has 17% MgO and would precipitate at the surface olivine with Fo 91.3. A unique melt fraction provides a unique primary magma solution, a successful mass balance solution to the primary magma problem. That is, the composition of the accumulated fractional melt (L) and the solid residue (S) for all major element oxide components is related to the initial peridotite composition by the mass balance equation: $C_o = FC_L + (1 - F)C_S$.

[86] Let us further explore the consequences of adding too much olivine to 1187-8.

[87] Case 5 is 1187-8 + 30% olivine (20% MgO): F in MgO-FeO space has no solution (Figure A1a). F = 0.32 in MgO-SiO_2 space (Figure A1b). F = 0.30 in projection space (Figure A1d). Composition 1187-8 + 30% olivine with 20% MgO cannot be a primary magma because there is no agreement among melt fractions. Now, MgO is too high for the liquid to be an accumulated fractional melt of our fertile peridotite source composition, and there is no solution for the melt fraction in MgO-FeO space.

[88] Diagrams that display primary magmas in MgO-SiO_2 or projection systematics are not by themselves very useful in constraining primary magma composition. However, their use together with MgO-FeO is very successful. Furthermore, the melt fraction isopleths in FeO-MgO space are accurate to with ±1% MgO, based on a ±1% uncertainty in K_D at the 1 σ level of confidence [*Herzberg and O'Hara*, 2002]. Also, a ±1% uncertainty in MgO would propagate to a large range in melt fraction, which can be independently evaluated with MgO-SiO_2 and projection systematics. For example, our primary magma composition with 17% MgO was determined by adding 19.5% olivine, yielding a consistency of 0.27 in melt fraction. Addition of 17% olivine drops MgO down to 16%, not much different. The 16% MgO melt would have a similar melt fraction in MgO-SiO_2 and projection space, but F would drop to

0.15 in MgO-FeO space (Table A1 and Figure A1), significantly lower than 0.27. The method is accurate because small variations in MgO propagate to large variations in melt fraction in MgO-FeO space. Furthermore, the accuracy increases substantially at lower FeO contents owing to the more restricted range of permitted MgO contents of primary magmas seen in Figure A1a. That is, there is a rough radial distribution to the melt fraction isopleths, and they become more compressed in MgO-FeO space at lower FeO contents. This is especially important for MORB as discussed in Figure 1a of the text.

A2. A Refresher on Forward Model Calculation

[89] As discussed immediately above, the forward model component provides a description of accumulated fractional melt compositions as functions of melt fraction. All diagrams used in this paper were originally produced and described by *Herzberg and O'Hara* [2002] and *Herzberg* [2004a], and the reader is referred to those papers for a comprehensive discussion of computational details. All melt fractions F in all figures used in this paper to constrain primary magma composition can be found in these references. Nevertheless, a few comments are now provided for those readers not familiar with that paper.

[90] *Herzberg and O'Hara* [2002] adopted two very different computational approaches to the calculation of an accumulated fractional melt composition, and obtained essentially identical results for F-FeO-MgO, which is the critical part of the forward model. The first solves Shaw's equations for accumulated fractional melting for any peridotite composition. Initially, liquid compositions are computed for [L + Ol] and [L + Ol + Opx] by mass balance solutions to the batch melting equation using an iterative procedure that incrementally varies F from 1.0 to about 0.24, where clinopyroxene becomes stable. These are based on experimentally based olivine-liquid distribution coefficients, which can be applied to any [L + Ol] and [L + Ol + Opx] assemblage. Liquid compositions in equilibrium with olivine (L + Ol) are solved for $X_{Opx} = 0$, and liquid compositions in equilibrium with harzburgite (L + Ol + Opx) are solved for $X_{Opx} = 0$ to a value that is also regulated by the stability of clinopyroxene (L + Ol + Opx + Cpx) where F is about 0.24. Results for equilibrium melting provide a unique value of D, the bulk distribution coefficient, for each value of melt fraction F. These are then substituted in *Shaw*'s [1970] equation for accumulated fractional melting to calculate the accumulated fractional melt composition.

[91] Shaw's equation yields FeO-MgO-F solutions that are very similar to those determined by the second method, the incremental batch procedure, which does require experimental an experimental database like KR-4003 from *Walter* [1998]. Briefly, a computation of the liquid composition was made of 0.01 mass fractions of equilibrium melting of the residue, and the liquid was perfectly removed from its residue. This fractional melting process changes the composition of each successive residue, which is melted again at 0.01 mass fractions of melting. Each liquid formed by 0.01 mass fractions of melting is called an instantaneous melt. Each new melt was perfectly extracted and mixed with the previously formed melt, and the mixture is the aggregate fractional melt. The compositions of FeO and MgO in the instantaneous melt produced at 0.01 mass fractions of melting were calculated from parameterizations of D for FeO as polybaric functions of the MgO content of the residue. In contrast to the first method, the calculations are performed iteratively for F that ranges from 0 to that at which Opx melts out. The results of this method provide an MgO-FeO-F diagram that is very similar to the first method which solves Shaw's equation; F is within 0.02 for specific MgO and FeO contents of accumulated fractional melts. However, it also provides information about the pressure of initial and final melting as shown in Figure A1.

[92] A third method has been developed for PRIMELT1 software construction. This is discussed below.

A3. A Practical Guide to Primary Magma Calculation

[93] Once the olivine addition array has been computed, the results can simply be layered on diagrams of the forward model from *Herzberg and O'Hara* [2002] and *Herzberg* [2004a]. This is the method we used in this paper. A melt fraction is read by visual inspection for each increment of olivine added, as discussed above. A unique melt fraction provides a unique primary magma solution. This is the most accurate method of obtaining primary magma composition. The problem, however, is that it is not convenient to use, although all diagrams that display melt fractions can be obtained from Herzberg on request, or they can

be constructed from solutions given in the electronic appendices of *Herzberg and O'Hara* [2002] and *Herzberg* [2004a]. Therefore PRIMELT1 software has been constructed that provides the same results to within 0.02 F.

A4. PRIMELT1 Software for Primary Magma Calculation

[94] We provide software entitled PRIMELT1 that is run with Microsoft Excel. A copy of PRIMELT1 (Software S1) is available in the auxiliary material[1]. PRIMELT1 calculates primary magma composition using melt fraction F as a constraint as discussed in section A1. The only input is the composition of a primitive lava composition that is representative of a set of lavas containing only olivine phenocrysts. Running PRIMELT1 with Ontong Java Plateau lava 1187-8 will replicate the results shown in Figure A1 and Table A1 to within 0.02 F and help the reader understand the computational method.

[95] First, for each liquid composition computed by olivine addition, F is computed for the case of batch melting by rearranging equations 22 and 23 of *Herzberg and O'Hara* [2002] to

$$F = (D_{FeO}MgO_L - 38.12K_D)/(D_{FeO}MgO_L - K_DMgO_L) \quad (A1)$$

where MgO_L is the wt % MgO content of the liquid, D_{FeO} is the bulk distribution coefficient for FeO, K_D is the FeO-MgO exchange coefficient at pressures within the melting regime [*Herzberg and O'Hara*, 2002], and 38.12 is the MgO content of fertile peridotite KR-4003. $F < 0$ when MgO in the liquid is lower than those for batch melts of fertile peridotite (Figure A2a). When $F > 0$, equation (A1) calculates FeO-MgO-F relations for batch melts exactly as they appear in Figure 4a of *Herzberg and O'Hara* [2002] and Figure A2a. Melt fractions in projection (Figure A1d) [*Herzberg and O'Hara*, 2002] have been parameterized with

$$F\ \text{projection} = 6.2819An^2 - 14.7789An^3 + 0.00825 \times (1/An)^2 \quad (A2)$$

where An refers to a projection coordinate as defined in the caption to Figure 2 in the text. Equations (A1) and (A2) permit the calculation of melt fraction for each liquid composition on the olivine addition array. A unique F provides a unique primary magma composition as described above in section A1. To calculate MgO for an accumulated fractional melt, we use Shaw's equation for each value of F and D for MgO obtained by mass balance for batch melting. The result is an approximation that usually overestimates MgO by a small amount (i.e., <1%); a correction appears in PRIMELT1 software. PRIMELT1 solutions for the MgO content of the accumulated fractional melt agree with those used throughout this paper and those reported by *Herzberg and O'Hara* [2002]; however, the melt fractions for which these solutions are obtained agree to within ±0.02.

[96] PRIMELT1 solves the primary magma composition for both batch and accumulated fractional melting of fertile peridotite KR-4003. As discussed in more detail below, the primary magma compositions will be similar to those for more depleted peridotite sources that have the same FeO content as KR-4003, which is about 8%. Later versions of the software will provide primary magma solutions for depleted peridotite compositions.

[97] PRIMELT1 will be most successful when the residue consists of spinel lherzolite, lherzolite, harzburgite, or dunite. However, PRIMELT1 will provide MgO contents that are about 2% too high if the residue consists of garnet peridotite. Peridotite-source melts from Hawaii are examples [*Herzberg*, 2006]; in this case, the most accurate method of obtaining primary magma composition is by graphically layering the olivine addition array (i.e., inverse model) on to diagrams that depict the primary magma compositions of fertile peridotite (i.e., forward model). This was the method used for Hawaii in Figure 3. A newer version of PRIMELT1 will eventually provide solutions for lavas extracted from garnet lherzolite residues.

[98] As this software was written from a parameterization of experimental results of *Walter* [1998], and as these experiments were anhydrous, primary magma solutions will only be useful for peridotite sources that contain low contents of H_2O, and melt to yield the magmas discussed in this paper (see section 4.0). There are many oceanic islands that were produced by wet melt extraction from a garnet lherzolite residue. A newer version of PRIMELT1 will eventually provide solutions for these cases.

[1]Auxiliary materials are available in the HTML. doi:10.1029/2006GC001390.

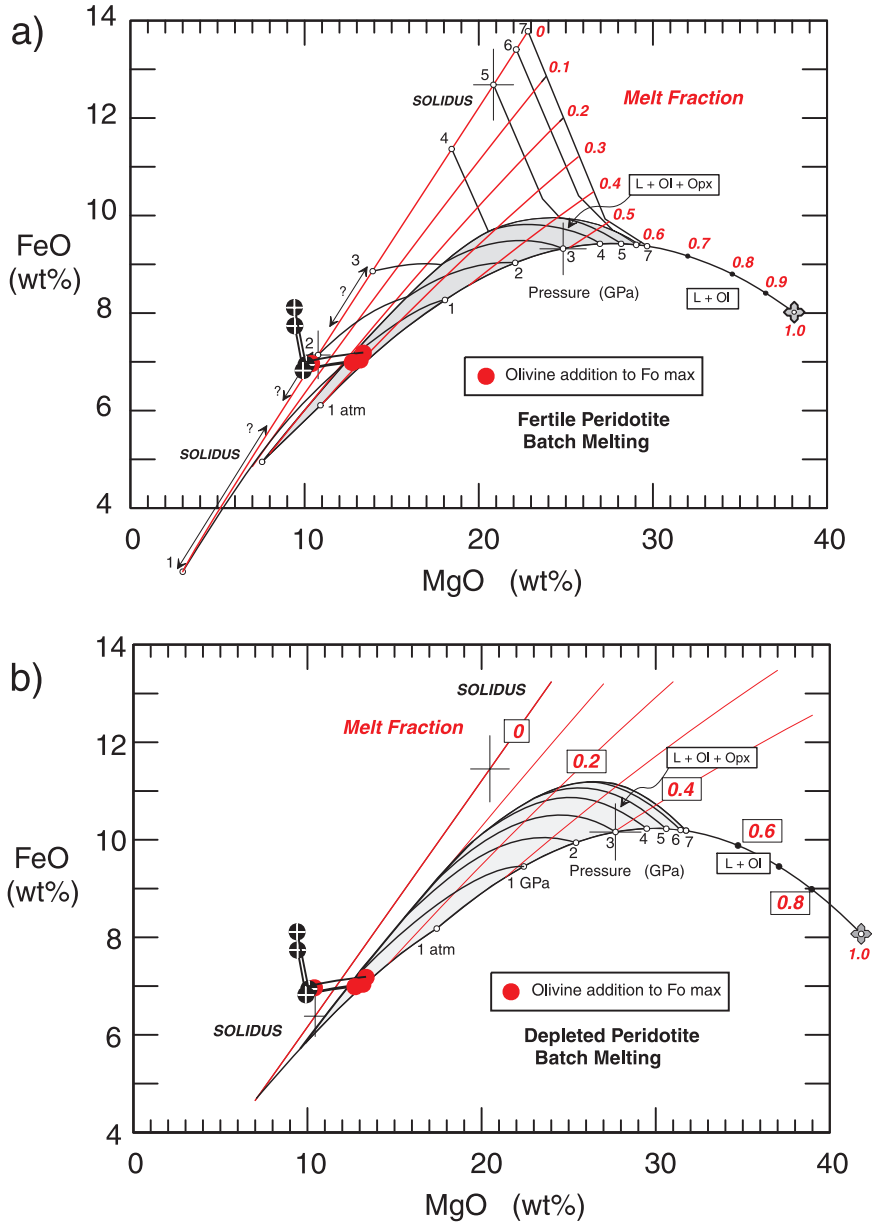

Figure A2. FeO and MgO contents of batch melts of peridotite [*Herzberg and O'Hara*, 2002; *Herzberg*, 2004a] compared with the four NMORB glass samples from Figure 6 and their parental magmas estimated by targeting to olivines with the maximum Fo contents. If these parental magmas were the same as the primary magmas, then the melt fractions would have to be about 0.25 and 0.15 for batch melting of fertile and depleted peridotite, respectively.

[99] PRIMELT1 will typically provide a primary magma composition for an erupted lava even if it formed from a pyroxenite source. In this case, the result is erroneous. Examples are primary magmas estimates for Kilauea [*Herzberg and O'Hara*, 2002], which are now erroneous because they formed from a pyroxenite source [*Herzberg*, 2006]. Progress is being made in distinguishing peridotite-source from pyroxenite-source lavas [*Herzberg*, 2006], and the results will eventually be incorporated into a newer version of PRIMELT1.

A5. Implications for Melting Conditions, Melt Productivity, and Crustal Thickness

[100] How does a model primary magma composition depend on the composition of the peridotite source? It was shown previously that it is negligible for mantle peridotite compositions with about

8% FeO [*Herzberg and O'Hara*, 2002], and this will be illustrated once again. Bulk compositions of fertile and depleted peridotite used in these calculations are given in Table A1, identical to the ones used by *Herzberg and O'Hara* [2002]. Additionally, we examine the consequences of deriving model MORB primary magmas by batch melting [*Green et al.*, 2001].

[101] The compositions of the primary magmas for Siqueiros MORB, Ontong Java Plateau, and Gorgona komatiites were estimated for a depleted peridotite composition in the text, and results were given in Figure 1a. Results of an assumed fertile source KR-4003 for OJP were shown above, and are extended to Sequeiros MORB and Gorgona komatiites, although not shown in Figure A1 for purposes of preserving clarity.

[102] For Ontong Java Plateau basalts, it was shown that the primary magma is targeted to a melt fraction of 0.27 in MgO-FeO, MgO-SiO_2, and projection space (Figure A1) yielding a primary accumulated OJP magma with 17% MgO. This is the same as we obtained for depleted peridotite (see text; see also *Herzberg* [2004c]). Although primary magma compositions are essentially the same for depleted and fertile peridotite sources, a large difference is revealed in the melt fractions, which are 0.11 for depleted peridotite and 0.27 for fertile peridotite. There is less mass of liquid obtained from depleted peridotite, although it is similar in composition.

[103] The NiO contents of Ontong Java Plateau basalts are, however, somewhat higher than those expected from differentiates of primary magmas derived from a peridotite source. They display similarities with NiO in some Hawaiian lavas, which crystallize olivines that are also high in NiO [*Sobolev et al.*, 2005]. One way to elevate NiO is by the production of a pyroxenite source that itself forms when peridotite reacts with partial melts of an eclogitic subducted crust [*Sobolev et al.*, 2005]. If indeed pyroxenite melting has played a role, the partial melts can be deficient in MgO compared to peridotite–source melts but, as discussed in section 7, inferred source temperatures can be too low [*Herzberg*, 2006]. However, a pyroxenite source might not be unique solution for the high NiO. For Ontong Java Plateau lavas, the successful mass balance solution to the primary magma problem for major elements points to the melting of a peridotite source. Magmatic NiO can become elevated during melt–rock reaction without exhaustion of olivine [*Kelemen et al.*, 1998]. This will further shown elsewhere for many cases of oceanic islands basalts.

[104] If indeed the Ontong Java Plateau lavas melted from a fertile peridotite source [*Fitton and Godard*, 2004; *Tejada et al.*, 2004, *Herzberg*, 2004c], the conditions of melting can be inferred from Figure A1. The green lines indicate how MgO, FeO, and SiO_2 change with decompression from various initial melting pressures; significant changes occur for FeO and SiO_2, but not for MgO. We can infer an initial melting pressure of ~3.5 GPa. The blue lines indicate the MgO, FeO, CaO, and SiO_2 compositions of the accumulated fractional melt at the pressure where melting stops. It is inferred to be 1.5 GPa from MgO-SiO_2 (Figure A1b) and MgO-CaO (Figure A1c), and about 1.7 GPa from MgO-FeO (Figure A1a). Although this level of agreement is extremely good, this slight misfit for FeO indicating that FeO might be about 0.1% too high. These pressures of final melting are substantially lower than pressures at the base of a mature lithosphere. The Ontong Java Plateau might be thick because melting extended through a thick melting column, and the fertile peridotite source melted extensively (F = 0.27). Whether these conditions of melting are unique to a mantle plume is a separate issue [*Fitton et al.*, 2004].

[105] For Gorgona komatiites, the primary magma from a fertile source is targeted to a melt fraction of 0.28 in both FeO-MgO and projection space. This primary accumulated Gorgona magma has 19% MgO, which compares with 19% obtained for depleted peridotite (see text).

[106] It is tempting to use Figure A1 to infer initial and final melting pressures for the Gorgona komatiites. However, these conditions are only valid if the source is fertile peridotite, in contrast to geochemical evidence which points to a depleted source [*Arndt et al.*, 1997]. Experimental data on depleted peridotite compositions at high pressure is necessary to obtain this pressure information, but these data are presently lacking.

[107] For MORB from the Siqueiros fracture zone, the primary magma is targeted to a melt fraction of 0.08 in FeO-MgO, SiO_2-MgO, and projection spaces, and the primary magma contains 12% MgO, only slightly lower than 13% for the depleted source (see text). Conditions of melting inferred from Figure A1 for fertile peridotite might be substantially in error if the source is depleted, as

indicated by trace element depletions [*Perfit et al.*, 1996].

[108] These examples demonstrate that uncertainties in the composition of a peridotite source do not propagate to large errors in MgO for computed primary magmas. In terms of obtaining primary magma MgO and temperature information, the method of calculation is very "forgiving." This result might not be intuitively obvious, but similar solutions are obtained for peridotite source compositions that have about 8% FeO. Indeed, the iron content for a wide range of fertile and depleted mantle peridotite remains at about 8%, similar to the iron content of MORB that is extracted [*Niu*, 1997; *Herzberg*, 2004c]. However, for Fe-rich peridotite sources having about 9% FeO, accumulated fractional melts will typically be lower in MgO by about 3% absolute [*Herzberg and O'Hara*, 2002].

[109] These examples demonstrate that it is very difficult to interpret the inferred melt fraction, unless there is some independent way of constraining the composition of the peridotite source. This will have a great impact on inferences concerning melt productivity and crustal thickness. Also, it is a good way to show that the temperature of a mantle plume cannot be inferred from the thickness of an oceanic plateau.

[110] Finally, we examine the commonly−made assumption that parental magmas calculated by inverting the process of fractional crystallization are similar to primary magmas produced by batch melting of peridotite [*Green et al.*, 2001]. Parental NMORB magmas from Figure 6 are compared with batch melts of fertile and depleted peridotite [*Herzberg and O'Hara*, 2002; *Herzberg*, 2004a] in Figure A2. For Siqueiros and Galapagos Rift MORB, back−tracking and targeting to olivines with Fo contents of 91.5–91.6, yields parental magmas with 13% MgO. If these parental magmas were the same as the primary magmas, then the melt fractions would have to be about 0.25 and 0.15 for batch melting of fertile and depleted peridotite, respectively (Figure A2). These melt fractions are too high because they would yield incompatible element abundances that are lower than observed [e.g., *Plank et al.*, 1995; *Workman and Hart*, 2005].

Acknowledgments

[111] We are very grateful to Don Anderson, Fred Frey, Dave Green, Marc Hirschmann, Charles Langmuir, Keith Putirka, Mike Rhodes, and three anonymous reviewers for critical reviews. We also thank Michael Baker for sharing experimental information and Francis Albarède for numerous discussions.

References

Agee, C. B. (1998), Crystal-liquid density inversions in terrestrial and lunar magmas, *Phys. Earth Planet. Inter.*, *107*, 63–74.

Aitken, B. G., and L. M. Echeverria (1984), Petrology and geochemistry of komatiites and tholeiites from Gorgona Island, Columbia, *Contrib. Mineral. Petrol.*, *86*, 94–105.

Albarède, F. (1992), How deep do common basaltic magmas form and differentiate?, *J. Geophys. Res.*, *97*, 10,997–11,009.

Albarède, F. (1995), *Introduction to Geochemical Modeling*, 543 pp., Cambridge Univ. Press, New York.

Albarède, F., B. Luais, G. Fitton, M. Semet, E. Kaminski, B. G. J. Upton, P. Bachèlery, and J.-L. Cheminée (1997), The geochemical regimes of Piton de la Fournaise volcano (Réunion) during the last 530000 years, *J. Petrol.*, *38*, 171–201.

Allen, R. M., et al. (1999), The thin hot plume beneath Iceland, *Geophys. J. Int.*, *137*, 51–63.

Anderson, D. L. (2000), The thermal state of the upper mantle: No role for mantle plumes, *Geophys. Res. Lett.*, *27*, 3623–3626.

Arndt, N. T. (1986a), Differentiation of komatiite flows, *J. Petrol.*, *27*, 279–301.

Arndt, N. T. (1986b), Komatiites: A dirty window to the Archean mantle, *Terra Cognita*, *6*, 59–66.

Arndt, N. T., A. C. Kerr, and J. Tarney (1997), Dynamic melting in plume heads: The formation of Gorgona komatiites and basalts, *Earth Planet. Sci. Lett.*, *146*, 289–301.

Arndt, N., C. Ginibre, C. Chauvel, F. Albarède, M. Cheadle, C. Herzberg, G. Jenner, and Y. Lahaye (1998), Were komatiites wet?, *Geology*, *26*, 739–742.

Asimow, P. D., and C. H. Langmuir (2003), The importance of water to oceanic mantle melting regimes, *Nature*, *421*, 815–820.

Asimow, P. D., and J. Longhi (2004), The significance of multiple saturation points in the context of polybaric near-fractional melting, *J. Petrol.*, *45*, 2349–2367.

Asimow, P. D., and E. M. Stolper (1999), Steady-state mantle-melt interactions in one dimension: 1. Equilibrium transport and melt focusing, *J. Petrol.*, *40*, 475–494.

Asimow, P. D., M. M. Hirschmann, and E. M. Stolper (2001), Calculation of peridotite partial melting from thermodynamic models of minerals and melts, IV. Adiabatic decompression and the composition and mean properties of mid-ocean ridge basalts, *J. Petrol.*, *42*, 963–998.

Asimow, P. D., J. E. Dixon, and C. H. Langmuir (2004), A hydrous melting and fractionation model for mid-ocean ridge basalts: Applications to the Mid-Atlantic Ridge near the Azores, *Geochem. Geophys. Geosyst.*, *5*, Q01E16, doi:10.1029/2003GC000568.

Barnes, S. J., R. E. T. Hill, and M. J. Gole (1988), The Perseverance ultramafic complex, western Australia: The product of a komatiite lava river, *J. Petrol.*, *29*, 305–331.

Beattie, P. (1993), Olivine-melt and orthopyroxene-melt equilibria, *Contrib. Mineral. Petrol.*, *115*, 103–111.

Bickle, M. J., A. Martin, and E. G. Nisbet (1975), Basaltic and peridotitic komatiites and stromatolites above a basal unconformity in the Belingwe Greenstone Belt, Rhodesia, *Earth Planet. Sci. Lett.*, *27*, 155–162.

Bickle, M. J., N. T. Arndt, E. G. Nisbet, J. L. Orpen, A. Martin, R. R. Keays, and R. Renner (1993), Geochemistry of the igneous rocks of the Belingwe greenstone belt: Alteration, contamination and petrogenesis, in *The Geology of the Belingwe Greenstone Belt, Zimbabwe*, edited by M. J. Bickle and E. G. Nisbet, pp. 175–213, A. A. Balkema, Brookfield, Vt.

Bowen, N. L. (1928), *The Evolution of the Igneous Rocks*, 332 pp., Princeton Univ. Press, Princeton, N. J.

Breddam, K. (2002), Kistufell: Primitive melt from the Iceland mantle plume, *J. Petrol.*, *43*, 345–373.

Bunge, H.-P. (2005), Low plume excess temperature and high core heat flux inferred from non-adiabatic geotherms in internally heated mantle circulation models, *Phys. Earth Planet. Inter.*, *153*, 3–10.

Campbell, I. H., and R. W. Griffiths (1990), Implications of mantle plume structure for the evolution of flood basalts, *Earth Planet. Sci. Lett.*, *99*, 79–83.

Cawthorn, R. G. (1975), Degrees of melting in mantle diapirs and the origin of ultrabasic liquids, *Earth Planet. Sci. Lett.*, *23*, 113–120.

Christie, D. M., I. S. E. Carmichael, and C. H. Langmuir (1986), Oxidation states of mid-ocean ridge basalt glasses, *Earth Planet. Sci. Lett.*, *79*, 397–411.

Clague, D. A., W. S. Weber, and J. E. Dixon (1991), Picritic glasses from Hawaii, *Nature*, *353*, 553–556.

Coogan, L. A., C. J. MacLeod, H. J. B. Dick, S. J. Edwards, A. Kvassnes, J. H. Natland, P. T. Robinson, G. Thompson, and M. J. O'Hara (2001), Whole-rock geochemistry of gabbros from the southwest Indian Ridge: Constraints on geochemical fractionations between the upper and lower oceanic crust and magma chamber processes at (very) slow-spreading ridges, *Chem. Geol.*, *178*, 1–22.

Danyushevsky, L. V. (2001), The effect of small amounts of H_2O on crystallisation of mid-ocean ridge and backarc basin magmas, *J. Volcanol. Geotherm. Res.*, *110*, 265–280.

Danyushevsky, L. V., S. M. Eggins, T. J. Falloon, and D. M. Christie (2000), H_2O abundance in depleted to moderately enriched mid-ocean ridge magmas; part I: Incompatible behaviour, implications for mantle storage, and origin of regional variations, *J. Petrol.*, *41*, 1329–1364.

Davies, J. H., and H.-P. Bunge (2006), Are splash plumes the origin of minor hotspots?, *Geology*, *34*, 349–352.

Davis, A. S., L. B. Gray, D. A. Clague, and J. R. Hein (2002), The Line Islands revisited: New $^{40}Ar/^{39}Ar$ geochronologic evidence for episodes of volcanism due to lithospheric extension, *Geochem. Geophys. Geosyst.*, *3*(3), 1018, doi:10.1029/2001GC000190.

Dixon, J. E., and D. A. Clague (2001), Volatiles in basaltic glasses from Loihi seamount, Hawaii: Evidence for a relatively dry plume component, *J. Petrol.*, *42*, 627–654.

Dixon, J. E., D. A. Clague, P. Wallace, and R. Poreda (1997), Volatiles in alkalic basalts from the North Arch volcanic field, Hawaii: Extensive degassing of deep submarine-erupted alkalic series lavas, *J. Petrol.*, *38*, 911–939.

Dixon, J. E., L. Leist, C. Langmuir, and J.-G. Schilling (2002), Recycled dehydrated lithosphere observed in plume-influenced mid-ocean-ridge basalt, *Nature*, *28*, 385–389.

Echeverria, L. M. (1980), Tertiary or Mesozoic komatiites from Gorgona Island, Columbia: Field relations and geochemistry, *Contrib. Mineral. Petrol.*, *73*, 253–266.

Echeverria, L. M., and B. G. Aitken (1986), Pyroclastic rocks: another manifestation of ultramafic volcanism on Gorgona Island, Columbia, *Contrib. Mineral. Petrol.*, *92*, 428–436.

Elthon, D. (1979), High magnesia liquids as the parental magma for ocean floor basalts, *Nature*, *278*, 514–518.

Elthon, D., D. K. Ross, and J. K. Meen (1995), Compositional variations of basaltic glasses from the Mid-Cayman Rise spreading center, *J. Geophys. Res.*, *100*, 12,497–12,512.

Falloon, T. J., and L. V. Danyushevsky (2000), Melting of refractory mantle at 1.5, 2 and 2.5 GPa under anhydrous and H_2O-undersaturated conditions: Implications for the petrogenesis of high-Ca boninites and the influence of subduction components on mantle melting, *J. Petrol.*, *41*, 257–283.

Farnetani, C. G., and H. Samuel (2005), Beyond the thermal plume paradigm, *Geophys. Res. Lett.*, *32*, L07311, doi:10.1029/2005GL022360.

Fitton, G. J., and M. Godard (2004), Origin and evolution of magmas on the Ontong Java Plateau, in *Origin and Evolution of the Ontong Java Plateau*, edited by J. G. Fitton et al., *Geol. Soc. Spec. Publ.*, *229*, 151–178.

Fitton, J. G., A. D. Saunders, P. D. Kempton, and B. S. Hardarson (2003), Does depleted mantle form an intrinsic part of the Iceland plume?, *Geochem. Geophys. Geosyst.*, *4*(3), 1032, doi:10.1029/2002GC000424.

Fitton, G. J., J. J. Mahoney, P. J. Wallace, and A. D. Saunders (2004), Origin and evolution of the Ontong Java Plateau: Introduction, in *Origin and Evolution of the Ontong Java Plateau*, edited by J. G. Fitton et al., *Geol. Soc. Spec. Publ.*, *229*, 1–8.

Ford, C. E., J. A. Russell, and M. R. Fisk (1983), Olivine-liquid equilibria: Temperature, pressure and composition dependence on the crystal/liquid cation partition coefficients for Mg, Fe^{2+}, Ca and Mn, *J. Petrol.*, *24*, 256–265.

Foulger, G. R., and J. H. Natland (2003), Is "hotspot" volcanism a consequence of plate tectonics?, *Science*, *300*, 921–922.

Foulger, G. R., et al. (2001), Seismic tomography shows that upwelling beneath Iceland is confined to the upper mantle, *Geophys. J. Int.*, *146*, 504–530.

Frey, F. A., M. O. Garcia, W. S. Wise, A. K. Kennedy, P. Gurriet, and F. Albarède (1991), The evolution of Mauna Kea volcano, Hawaii: Petrogenesis of tholeiitic and alkalic basalts, *J. Geophys. Res.*, *96*, 14,347–14,375.

Fyfe, W. S. (1978), The evolution of the Earth's crust: Modern plate tectonics to ancient hot spot tectonics?, *Chem. Geol.*, *23*, 89–114.

Gast, P. W. (1968), Trace element fractionation and the origin of tholeiitic and alkaline magma types, *Geochim. Cosmochim. Acta*, *32*, 1057–1086.

Ghiorso, M. S., and R. O. Sack (1995), Chemical mass transfer in magmatic processes, IV, A revised and internally consistent thermodynamic model for the interpolation and extrapolation of liquid-solid equilibria in magmatic systems at elevated temperatures and pressures, *Contrib. Mineral. Petrol.*, *119*, 197–212.

Green, D. H., W. O. Hibberson, and A. L. Jaques (1979), Petrogenesis of mid-ocean ridge basalts, in *The Earth: Its Origin, Structure and Evolution*, edited by M. W. McElhinny, pp. 265–290, Elsevier, New York.

Green, D. H., T. J. Falloon, S. M. Eggins, and G. M. Yaxley (2001), Primary magmas and mantle temperatures, *Eur. J. Mineral.*, *13*, 437–451.

Grove, T. L., and W. B. Bryan (1983), Fractionation of pyroxene-phyric MORB at low pressure: An experimental study, *Contrib. Mineral. Petrol.*, *84*, 293–309.

Grove, T. L., R. J. Kinzler, and W. B. Bryan (1992), Fractionation of mid-ocean ridge basalt (MORB), in *Mantle Flow and Melt Generation at Mid-Ocean Ridges*, *Geophys. Monogr. Ser.*, vol. 71, edited by J. P. Morgan, D. K. Blackman, and J. M. Sinton, pp. 281–310, AGU, Washington, D. C.

Hanson, G. N., and C. H. Langmuir (1978), Modelling of major elements in mantle-melt systems using trace element approaches, *Geochim. Cosmochim. Acta*, *42*, 725–741.

Herzberg, C. (2004a), Geodynamic information in peridotite petrology, *J. Petrol.*, *45*, 2507–2530.

Herzberg, C. (2004b), Partial crystallization of mid-ocean ridge basalts in the crust and mantle, *J. Petrol.*, *45*, 2389–2405.

Herzberg, C. (2004c), Partial melting below the Ontong Java Plateau, in *Origin and Evolution of the Ontong Java Plateau*, edited by J. G. Fitton et al., *Geol. Soc. Spec. Publ.*, *229*, 179–183.

Herzberg, C. (2006), Petrology and thermal structure of the Hawaiian plume from Mauna Kea volcano, *Nature*, *444*, 605–609.

Herzberg, C., and M. J. O'Hara (2002), Plume-associated ultramafic magmas of Phanerozoic age, *J. Petrol.*, *43*, 1857–1883.

Irvine, T. N. (1977), Definition of primitive liquid compositions for basic magmas, *Carnegie Inst. Wash. Year Book*, *76*, 454–461.

Jarvis, G. T., and I. H. Campbell (1983), Archean komatiites and geotherms: Solution to an apparent contradiction, *Geophys. Res. Lett.*, *10*, 1133–1136.

Johnson, K. T. M., H. J. B. Dick, and N. Shimizu (1990), Melting in the oceanic upper mantle: An ion microprobe study of diopsides in abyssal peridotites, *J. Geophys. Res.*, *95*, 2661–2678.

Karato, S.-I. (2004), Mapping water content in the upper mantle, in *Inside the Subduction Factory*, *Geophys. Monogr. Ser.*, vol. 138, edited by J. Eiler, pp. 135–152, AGU, Washington, D. C.

Kareem, K. M., and G. R. Byerly (2003), Petrology and geochemistry of 3.3 Ga Komatiites—Weltevreden Formation, Barberton greenstone belt, paper presented at the 34th Lunar and Planetary Science Conference, Lunar and Planet. Inst., League City, Tex.

Kelemen, P. B., G. Hirth, N. Shimizu, M. Spiegelman, and H. J. B. Dick (1997), A review of melt migration processes in the asthenospheric mantle beneath oceanic spreading centers, *Philos. Trans. R. Soc. London, Ser. A*, *355*, 283–318.

Kelemen, P. B., S. R. Hart, and S. Bernstein (1998), Silica enrichment in the continental upper mantle via melt/rock reaction, *Earth Planet. Sci. Lett.*, *164*, 387–406.

Kempton, P. D., J. G. Fitton, A. D. Saunders, G. M. Nowell, R. N. Taylor, B. S. Hardarson, and G. Pearson (2000), The Iceland plume in space and time: A Sr-Nd-Pb-Hf study of the North Atlantic rifted margin, *Earth Planet. Sci. Lett.*, *177*, 255–271.

Kerr, A. C., G. F. Marriner, N. T. Arndt, J. Tarney, A. Nivia, A. D. Saunders, and R. A. Duncan (1996), The petrogenesis of Gorgona komatiites, picrites and basalts: New field, petrographic and geochemical constraints, *Lithos*, *37*, 245–260.

Kinzler, R. (1997), Melting of mantle peridotite at pressures approaching the spinel to garnet transition: Application to mid-ocean ridge basalt petrogenesis, *J. Geophys. Res.*, *102*, 853–874.

Kinzler, R., and T. L. Grove (1992), Primary magmas of mid-ocean ridge basalts: 2. Applications, *J. Geophys. Res.*, *97*, 6907–6926.

Klein, E. M., and C. H. Langmuir (1987), Global correlations of ocean ridge basalt chemistry with axial depth and crustal thickness, *J. Geophys. Res.*, *92*, 8089–8115.

Kogiso, T., M. M. Hirschmann, and M. Pertermann (2004), High-pressure partial melting of mafic lithologies in the mantle, *J. Petrol.*, *45*, 2407–2422.

Lahaye, Y., and N. Arndt (1996), Alteration of a komatiite flow from Alexo, Ontario, Canada, *J. Petrol.*, *37*, 1261–1284.

Langmuir, C. H., and G. N. Hanson (1980), An evaluation of major element heterogeneity in the mantle sources of basalts, *Philos. Trans. R. Soc. London, Ser. A*, *297*, 383–407.

Langmuir, C. H., E. M. Klein, and T. Plank (1992), Petrological systematics of mid-ocean ridge basalts: Constraints on melt generation beneath ocean ridges, in *Mantle Flow and Melt Generation at Mid-Ocean Ridges*, *Geophys. Monogr. Ser.*, vol. 71, edited by J. P. Morgan, D. K. Blackman, and J. M. Sinton, pp. 183–280, AGU, Washington, D. C.

Larsen, L. M., and A. K. Pedersen (2000), Processes in high-Mg, high-T magmas: Evidence from olivine, chromite and glass in Palaeogene picrites from West Greenland, *J. Petrol.*, *41*, 1071–1098.

Lesher, C. M., and N. T. Arndt (1995), REE and Nd isotope geochemistry, petrogenesis and volcanic evolution of contaminated komatiites at Kambalda, western Australia, *Lithos*, *34*, 127–157.

Lesher, C. M., and D. I. Groves (1986), Controls on the formation of komatiite-associated nickel-copper sulfide deposits, in *Geology and Metallogeny of Copper Deposits*, edited by G. H. Friedrich et al., pp. 43–62, Springer, New York.

Lewis, J. D., and J. R. Williams (1973), The petrology of an ultramafic lava near Murphy Well, Eastern Goldfields, western Australia, *Annu. Rep. 60-68*, Geol. Surv. of West. Aust., East Perth.

Lewis, J. V. (1907), Petrography of the Newark Igneous Rocks of New Jersey, in *Annual Report of the State Geologist, Part IV*, pp. 97–167, N. J. Geol. Surv., Trenton.

Lin, S.-C., and P. E. van Keken (2005), Multiple volcanic episodes of flood basalts caused by thermochemical mantle plumes, *Nature*, *436*, 250–252.

Loper, D. E., and F. D. Stacey (1983), The dynamical and thermal structure of deep mantle plumes, *Phys. Earth Planet. Inter.*, *33*, 304–317.

Maclennan, J., D. McKenzie, and K. Gronvöld (2001), Plume-driven upwelling under central Iceland, *Earth Planet. Sci. Lett.*, *194*, 67–82.

Maclennan, J., D. McKenzie, K. Grönvold, N. Shimizu, J. M. Eiler, and N. Kitchen (2003), Melt mixing and crystallization under Theistareykir, northeast Iceland, *Geochem. Geophys. Geosyst.*, *4*(11), 8624, doi:10.1029/2003GC000558.

McDonough, W. F., and S.-S. Sun (1995), The composition of the Earth, *Chem. Geol.*, *120*, 223–253.

McKenzie, D. (1984), The generation and compaction of partial melts, *J. Petrol.*, *25*, 713–765.

McKenzie, D. (2000), Constraints on melt generation and transport from U-series activity ratios, *Chem. Geol.*, *162*, 81–94.

McKenzie, D., and M. J. Bickle (1988), The volume and composition of melt generated by extension of the lithosphere, *J. Petrol.*, *29*, 625–679.

McKenzie, D., and R. K. O'Nions (1991), Partial melt distributions from inversion of rare-earth element concentrations, *J. Petrol.*, *32*, 1021–1091.

McKenzie, D., J. Jackson, and K. Priestley (2005), Thermal structure of oceanic and continental lithosphere, *Earth Planet. Sci. Lett.*, *233*, 337–349.

McNeill, A. W., and L. V. Danyushevsky (1996), Composition and crystallization temperatures of primary melts from Hole 896A basalts: Evidence from melt inclusion studies, *Proc. Ocean Drill. Program Sci. Results*, *148*, 21–35.

Michael, P. J. (1995), Regionally distinctive sources of depleted MORB: Evidence from trace elements and H_2O, *Earth Planet. Sci. Lett.*, *131*, 301–320.

Michael, P. J. (1999), Implications for magmatic processes at Ontong Java Plateau from volatile and major element contents of Cretaceous basalt glasses, *Geochem. Geophys. Geosyst.*, *1*(1), doi:10.1029/1999GC000025.

Montelli, R., G. Nolet, F. A. Dahlen, G. Masters, E. R. Engdahl, and S. H. Hung (2004), Finite-frequency tomography reveals a variety of plumes in the mantle, *Science*, *303*, 338–343.

Morgan, W. J. (1971), Convection plumes in the lower mantle, *Nature*, *230*, 42–43.

Murata, K. J., and D. H. Richter (1966), Chemistry of the lavas of the 1959–1960 eruption of Kilauea volcano, Hawaii, *U. S. Geol. Surv. Prof. Pap.*, *537-A*, 1–26.

Nichols, A. R. L., M. R. Carroll, and A. Höskuldsson (2002), Is the Iceland hot spot also wet? Evidence from the water contents of undegassed submarine and subglacial pillow basalts, *Earth Planet. Sci. Lett.*, *202*, 77–87.

Nisbet, E. G., M. J. Bickle, and A. Martin (1977), The mafic and ultramafic lavas of the Belingwe Greenstone Belt, S. Rhodesia, *J. Petrol.*, *18*, 521–566.

Nisbet, E. G., N. T. Arndt, M. J. Bickle, W. E. Cameron, C. Chauvel, M. Cheadle, A. Hegner, A. Martin, R. Renner, and E. Roedder (1987), Uniquely fresh 2.7 Ga old komatiites from the Belingwe Greenstone Belt, Zimbabwe, *Geology*, *15*, 1147–1150.

Nisbet, E. G., M. J. Cheadle, N. T. Arndt, and M. J. Bickle (1993), Constraining the potential temperature of the Archean mantle: A review of the evidence from komatiites, *Lithos*, *30*, 291–307.

Niu, Y. (1997), Mantle melting and melt extraction processes beneath ocean ridges: Evidence from abyssal peridotites, *J. Petrol.*, *38*, 1047–1074.

Niu, Y., and R. Batiza (1991), An empirical method for calculating melt compositions produced beneath mid-ocean ridges: Application for axis and off-axis (seamounts) melting, *J. Geophys. Res.*, *96*, 21,753–21,777.

Norman, M. C., and M. O. Garcia (1999), Primitive magmas and source characteristics of the Hawaiian plume: Petrology and geochemistry of shield picrites, *Earth Planet. Sci. Lett.*, *168*, 27–44.

O'Hara, M. J. (1968), Are ocean floor basalts primary magmas?, *Nature*, *220*, 683–686.

O'Hara, M. J., and H. S. Yoder, Jr. (1967), Formation and fractionation of basic magmas at high pressures, *Scot. J. Geol.*, *3*, 67–117.

Pearce, T. H. (1978), Olivine fractionation equations for basaltic and ultrabasic liquids, *Nature*, *276*, 771–774.

Perfit, M. R., D. J. Fornari, W. I. Ridley, P. D. Kirk, J. Casey, K. A. Kastens, J. R. Reynolds, M. Edwards, D. Desonie, R. Shuster, and S. Paradis (1996), Recent volcanism in the Siqueiros transform fault: Picritic basalts and implications for MORB magma genesis, *Earth Planet. Sci. Lett.*, *141*, 91–108.

Pertermann, M., and M. M. Hirschmann (2003), Anhydrous partial melting experiments on MORB-like eclogite: Phase relations, phase compositions and mineral-melt partitioning of major elements at 2–3 GPa, *J. Petrol.*, *44*, 2173–2201.

Plank, T., M. Spiegelman, C. H. Langmuir, and D. W. Forsyth (1995), The meaning of "mean F": Clarifying the mean extent of melting at oceanic ridges, *J. Geophys. Res.*, *100*, 15,045–15,052.

Pollack, H. N. (1997), Thermal characteristics of the Archaean, in *Greenstone Belts*, *Oxford Monogr. Geol. Geophys.*, vol. 35, edited by M. de Wit and L. D. Ashwall, pp. 223–232, Clarendon, Oxford, U. K.

Presnall, D. C., and J. D. Hoover (1987), High pressure phase equilibrium constraints on the origin of mid-ocean ridge basalts, *Geochem. Soc. Spec. Publ.*, *1*, 75–89.

Presnall, D. C., G. H. Gudfinnson, and M. J. Walter (2002), Generation of mid-ocean ridge basalts at pressures from 1 to 7 GPa, *Geochim. Cosmochim. Acta*, *66*, 2073–2090.

Putirka, K. D. (2005), Mantle potential temperatures at Hawaii, Iceland, and the mid-ocean ridge system, as inferred from olivine phenocrysts: Evidence for thermally driven mantle plumes, *Geochem. Geophys. Geosyst.*, *6*, Q05L08, doi:10.1029/2005GC000915.

Putirka, K. D., M. Perfit, and F. J. Ryerson (2006), Ambient and excess mantle temperatures, olivine thermometry, and active vs. passive upwelling, *Chem. Geol.*, in press.

Révillon, S., N. T. Arndt, E. Hallot, A. C. Kerr, and J. Tarney (1999), Petrogenesis of picrites from the Caribbean plateau and the North Atlantic magmatic province, *Lithos*, *49*, 1–21.

Révillon, S., N. T. Arndt, C. Chauvel, and E. Hallot (2000), Geochemical study of ultramafic volcanic and plutonic rocks from Gorgona Island, Colombia: The plumbing system of an oceanic plateau, *J. Petrol.*, *41*, 1127–1153.

Rhodes, J. M., and M. J. Vollinger (2005), Ferric/ferrous ratios in 1984 Mauna Loa lavas: A contribution to understanding the oxidation state of Hawaiian magmas, *Contrib. Mineral. Petrol.*, *149*, 666–674.

Rhodes, J. M., M. A. Dungan, D. P. Blanchard, and P. E. Long (1979), Magma mixing at mid-ocean ridges: Evidence from basalts drilled near 22°N on the Mid-Atlantic Ridge, *Tectonophysics*, *55*, 35–61.

Ribe, N. M. (1985), The generation and composition of partial melts in the Earth's mantle, *Earth Planet. Sci. Lett.*, *73*, 361–376.

Richter, F. M. (1986), Simple models for trace element fractionation during melt segregation, *Earth Planet. Sci. Lett.*, *77*, 333–344.

Roberge, J., R. V. White, and P. J. Wallace (2004), Volatiles in submarine basaltic glasses from the Ontong Java Plateau (ODP Leg 192): Implications for magmatic processes and source regions compositions, in *Origin and Evolution of the Ontong Java Plateau*, edited by J. G. Fitton et al., *Geol. Soc. Spec. Publ.*, *229*, 239–257.

Roeder, P. L., and R. F. Emslie (1970), Olivine-liquid equilibrium, *Contrib. Mineral. Petrol.*, *29*, 275–289.

Sano, T., and S. Yamashita (2004), Experimental petrology of basement lavas from Ocean Drilling Program Leg 192: Implications for differentiation processes in Ontong Java Plateau magmas, in *Origin and Evolution of the Ontong Java Plateau*, edited by J. G. Fitton et al., *Geol. Soc. Spec. Publ.*, *229*, 185–218.

Saunders, A. D. (2005), Large igneous provinces: Origin and environmental consequences, *Elements*, *1*, 259–263.

Saunders, A. D., J. G. Fitton, A. C. Kerr, M. J. Norry, and R. W. Kent (1997), The North Atlantic igneous province, in *Large Igneous Provinces: Continental, Oceanic, and Planetary Flood Volcanism*, *Geophys. Monogr. Ser.*, vol. 100, edited by J. J. Mahoney and M. J. Coffin, pp. 45–93, AGU, Washington, D. C.

Schilling, J.-G. (1991), Fluxes and excess temperatures of mantle plumes inferred from their interaction with migrating mid-ocean ridges, *Nature*, *352*, 397–403.

Schubert, G., G. Masters, P. Olson, and P. Tackley (2004), Superplumes or plume clusters?, *Phys. Earth Planet. Inter.*, *146*, 147–162.

Schwartz, J. J., B. E. John, M. J. Cheadle, E. A. Miranda, C. B. Grimes, J. L. Wooden, and H. J. B. Dick (2005), Dating the growth of oceanic crust at a slow-spreading center, *Science*, *310*, 654–657.

Shaw, D. M. (1970), Trace element fractionation during anatexis, *Geochim. Cosmochim. Acta*, *34*, 237–243.

Shen, Y., and D. W. Forsyth (1995), Geochemical constraints on initial and final depths of melting beneath mid-ocean ridges, *J. Geophys. Res.*, *100*, 2211–2237.

Slater, L., D. McKenzie, K. Grönvold, and N. Shimizu (2001), Melt generation and movement beneath Theistareykir, NE Iceland, *J. Petrol.*, *42*, 321–354.

Sobolev, A. V., and M. Chassidon (1996), H_2O concentrations in primary melts from supra-subduction zones and mid-ocean ridges: Implications for H_2O storage and recycling in the mantle, *Earth Planet. Sci. Lett.*, *137*, 45–55.

Sobolev, A. V., and I. K. Nikogosian (1994), Petrology of long-lived mantle plume magmatism: Hawaii, Pacific and Reunion island, Indian Ocean, *Petrology*, *2*, 111–144.

Sobolev, A. V., A. W. Hofmann, S. V. Sobolev, and I. K. Nikogosian (2005), An olivine-free mantle source of Hawaiian shield basalts, *Nature*, *434*, 590–597.

Spiegelman, M., and T. Elliott (1993), Consequences of melt transport for uranium series disequilibrium in young lavas, *Earth Planet. Sci. Lett.*, *118*, 1–20.

Sproule, R. A., C. M. Lesher, J. A. Ayer, P. C. Thurston, and C. T. Herzberg (2002), Spatial and temporal variations in the geochemistry of komatiites and komatiitic basalts in the Abitibi greenstone belt, *Precambrian Res.*, *115*, 153–186.

Tejada, M. L. G., J. J. Mahoney, P. R. Castillo, S. P. Ingle, H. C. Sheth, and D. Weiss (2004), Pin-pricking the elephant (ODP Leg 192): Pb-Sr-Hf-Nd isotopic evidence on the origin of the Ontong Java Plateau, in *Origin and Evolution of the Ontong Java Plateau*, edited by J. G. Fitton et al., *Geol. Soc. Spec. Publ.*, *229*, 133–150.

Thirlwall, M. R., M. A. M. Gee, R. N. Taylor, and B. J. Murton (2004), Mantle components in Iceland and adjacent ridges investigated using double-spike Pb isotope ratios, *Geochim. Cosmochim. Acta*, *68*, 361–386.

Toplis, M. J. (2005), The thermodynamics of iron and magnesium partitioning between olivine and liquid: Criteria for assessing and predicting equilibrium in natural and experimental systems*Contrib. Mineral. Petrol.*, *149*, 22–39.

Walter, M. J. (1998), Melting of garnet peridotite and the origin of komatiite and depleted lithosphere, *J. Petrol.*, *39*, 29–60.

Watson, S., and D. McKenzie (1991), Melt generation by plumes: A study of Hawaiian volcanism, *J. Petrol.*, *32*, 501–537.

Werner, R., K. Hoernle, U. Barckhausen, and F. Hauff (2003), Geodynamic evolution of the Galápagos hot spot system (Central East Pacific) over the past 20 m.y.: Constraints from morphology, geochemistry, and magnetic anomalies, *Geochem. Geophys. Geosyst.*, *4*(12), 1108, doi:10.1029/2003GC000576.

White, R. S., and D. McKenzie (1989), Magmatism at rift zones: The generation of volcanic continental margins and flood basalts, *J. Geophys. Res.*, *94*, 7685–7729.

White, W. M., A. R. McBirney, and R. A. Duncan (1993), Petrology and geochemistry of the Galapagos Islands: Portrait of a pathological mantle plume, *J. Geophys. Res.*, *98*, 19,533–19,563.

Wilson, J. T. (1963), A possible origin of the Hawaiian Islands, *Can. J. Earth Sci.*, *41*, 863–870.

Workman, R. K., and S. R. Hart (2005), Major and trace element composition of the depleted MORB mantle (DMM), *Earth Planet. Sci. Lett.*, *231*, 53–72.

Wright, T. (1972), Chemistry of Kilauea and Mauna Loa lava in space and time, *U.S. Geol. Surv. Prof. Pap.*, *735*, 1–39.

Wright, T. (1973), Magma mixing as illustrated by the 1959 eruption, Kilauea Volcano, Hawaii, *Geol. Soc. Am. Bull.*, *84*, 849–858.

Wright, T., and R. S. Fiske (1971), Origin of the differentiated and hybrid lavas of Kilauea Volcano, Hawaii, *J. Petrol.*, *12*, 1–65.

Wright, T., D. A. Swanson, and W. A. Duffield (1975), Chemical compositions of Kilauea east-rift lava, 1968–1971, *J. Petrol.*, *16*, 110–133.

Yang, H.-J., R. J. Kinzler, and T. L. Grove (1996), Experiments and models of anhydrous, basaltic olivine-plagioclase-augite saturated melts from 0.001 to 10 kbar, *Contrib. Mineral. Petrol.*, *124*, 1–18.

Yasuda, A., T. Fujii, and K. Kurita (1994), Melting phase relations of an anhydrous mid-ocean ridge basalt from 3 to 20 GPa: Implications for the behavior of subducted oceanic crust in the mantle, *J. Geophys. Res.*, *99*, 9401–9414.

Yaxley, G. M., and D. H. Green (1998), Reactions between eclogite and peridotite: Mantle refertilisation by subduction of oceanic crust, *Schweiz. Mineral. Petrogr. Mitt.*, *78*, 243–255.